Spatial and Temporal Variability of Double Diffusive Structures in Powell Lake, British Columbia

by

Artem Zaloga

B. Sc. Engineering Physics, Queen's University, 2013

A THESIS SUBMITTED IN PARTIAL FULFILLMENT
OF THE REQUIREMENTS FOR THE DEGREE OF

Master of Science

in

THE FACULTY OF GRADUATE AND POSTDOCTORAL STUDIES
(Oceanography)

The University of British Columbia
(Vancouver)

December 2015

Abstract

The spatial and temporal properties of naturally occurring double diffusive (DD) structures present in the bottom waters of Powell Lake, British Columbia were investigated. Observations were obtained from four annual surveys consisting of vertical cm-resolution conductivity-temperature-depth (CTD) profiles along the 9 km length of the lake, and from a month-long mooring consisting of thirty-eight temperature sensors and two current meters.

DD layers were identified by isolating clusters on T-S diagrams, and tracked spatially and temporally throughout each of the CTD surveys. The layers were observed to be persistent over four years, and horizontally coherent over the entire lake length at depths of 336-347 m. In this region the vertical density ratio and buoyancy frequency were near constant at $R_{\rho z} = 2.2 \pm 0.2$ and $N = (2.3 \pm 0.3) \times 10^{-3}$ Hz, and the Rayleigh number reached a peak at $Ra \approx 10^7$. Layers just above and below this region were less horizontally-coherence and with larger values of $R_{\rho z}$ and N.

Spatial variations in layer depth and the background temperature/salinity distribution showed persistent trends throughout the study period. These trends indicated that layer slope and horizontal property gradients are linked and that the horizontal density ratio, $R_{\rho x}$, may be an indicator of the mean layer slope. Linear fits to the layer properties indicated that a horizontal density ratio of $R_{\rho x} = -0.35 \pm 0.17$ was accompanied by a mean layer slope of $\Delta z/\Delta x = 0.05 \pm 0.02$ m/km.

An individual DD step within one of the stable and horizontally coherent DD layers was identified within the moored temperature time series and tracked over the course of a week. The convective regime within the DD step was observed to be composed of intermittent thermal plumes emitted from the bottom diffusive interface. The features appeared as a common peak in the mean DD step temperature and horizontal velocity power spectra. The plumes had a period of ~ 22 minutes (a factor of 3 greater than the buoyancy period), a temperature scale of $T' \approx 0.2$ m°C, and horizontal and vertical velocity scales of $u' = w' \approx 0.5$ mm/s.

Preface

This thesis is original and unpublished work carried out by the author, Artem Zaloga, under the supervision of Richard Pawlowicz. CTD surveys during the years of 2012 and 2013 were conducted by Benjamin Scheifele and Richard Pawlowicz, and during the years of 2014 and 2015 by the author, alone and with Richard Pawlowicz. The mooring was designed and built by the author with the assistance of Roger Pieters and Steve Pond. All field work was conducted with the assistance of the sea-going technicians, Chris Payne and Larysa Pakhomova. Figure 2.1 and Figure 4.2 are adapted with permission from Scheifele et al. (2014) and Turner and Chen (1974) respectively.

Table of Contents

List of Figures

Acknowledgments

I would like to thank

Stephanie Waterman, Gregory Lawrence, and Susan Allen for taking the time to edit this work; Roger Pieters and Steven Pond for the immense amount of assistance with all of the instruments; Chris Payne and Larysa Pakhomova for the tireless hours spent sampling on that damn lake.

I would also like to specifically thank my supervisor, Richard Pawlowicz, for the countless hours spent helping me throughout this work and, in effect, stretching the boundaries of my mind.

And I would like to thank my dear friends and family for ensuring that those boundaries didn't drift into insanity... too often. How you put up with me, I've no idea.

Dedication

To Charlie.

Chapter 1

Introduction and Background

In an oceanographic setting, the dynamically important aspects of the density of water are primarily determined by the salt content and temperature of the water. In the case where the overall vertical density gradient is gravitationally stable but either one of temperature or salinity have an unstable vertical gradient, the very different molecular diffusivities of heat and salt can give rise to a class of instabilities known as double diffusive instabilities.

Via molecular diffusion, these instabilities transfer the potential energy stored in the unstable gradient into convective motions within the water column; convective motions which themselves have a tendency to organize into large scale structures within the ocean and many lakes. These structures can cover large horizontal areas, and although their importance for the global ocean circulation is uncertain (Ruddick and Gargett, 2003), their existence is observed in many parts of the ocean, especially in the Arctic. The purpose of this work is to further investigate the spatial and temporal properties of these structures in a natural environment, in order to compare with previous laboratory and numerical studies, as well as to better predict their effects on the vertical transport of heat and salt within the ocean.

1.1 The Double Diffusive Instability

Even if the overall density gradient of a water mass is gravitationally stable (increasing monotonically with depth) it may still be susceptible to convective instabilities if either the salinity or temperature gradients of the water mass are unstably stratified. This is due to the fact that the molecular diffusivity of heat is greater than that of salt by a factor of about 100, which results in temperature gradients evolving at a more rapid rate than those of salt. Under certain circumstances this may create regions with small buoyant instabilities, so that the potential energy stored up in the destabilizing gradient is partially converted into convective motions via these instabilities. This phenomenon was first proposed theoretically by Stern (1960), and is now described by the term double diffusive convection.

There are two possible arrangements of salinity and temperature gradients (with one stabilizing and the other destabilizing the system) that create a stable density profile – resulting in two different

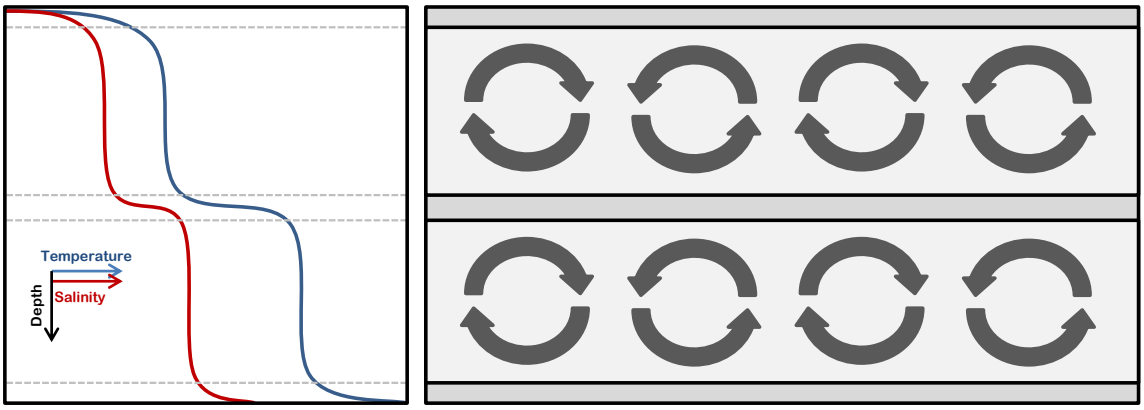

Figure 1.1: Left to right: An example of the characteristic staircase structure observed in vertical profiles of temperature (blue) and salinity (red) within the diffusive layering regime; the associated schematic depicting the convective regions (dark grey eddies) and diffusive interfaces (empty grey).

instability modes. The first occurs when both gradients decrease monotonically with depth, producing a stabilizing temperature gradient and destabilizing salinity gradient; the second occurs when both gradients increase with depth, producing temperature and salinity gradients with the converse effects. The former mode is called 'Salt Fingering' due to the propensity of the instabilities to develop as vertical, finger-like protrusions; the latter mode is called 'Diffusive Layering' due to the observation of these instabilities primarily after they have evolved into a layered structure.

In the ocean, the salt fingering mode is dominant in mid-latitudes (Kunze, 2003) where warm, salty waters overlie colder, fresher waters, whereas the diffusive layering mode is dominant in high-latitude regions (Kelley et al., 2003) where cold, fresh waters overlie warmer, saltier waters. In both cases, the instabilities can be identified because of a common feature observed in both modes: they have a tendency to evolve into stacks of horizontal layers which are observed as staircase structures in vertical temperature and salinity profiles (Figure 1.1, left). These layers are composed of water masses with differing, but still gravitationally stable, densities, and the resulting staircase structure is considered an indicator of double diffusive instabilities.

Schematically, these layers are understood to consist of 'convective regions' ('risers' in the staircases) with near uniform properties, sandwiched vertically between 'diffusive interfaces' ('treads' in the staircases) with high gradients of both temperature and salinity (Figure 1.1, right). As the terms imply, fluxes in the convective regions are governed by active convection, and fluxes through the diffusive interfaces are thought to be governed by molecular diffusion only.

The present work is concerned solely with the diffusive layering mode of the instability, but the interested reader is referred to the reviews by Kunze (2003) and Radko (2013) for further reading into the salt fingering mode of the instability.

1.2 Laboratory Observations

The original stability analysis of linear gradients of temperature and salinity presented by Stern (1960) focused mainly on the salt fingering mode and left the diffusive layering mode to a mere footnote. However, due to the symmetry of the equations for the two modes (one needs only to change the signs on the assumed temperature and salinity gradients to go from one mode to the other), the main conclusion equally applies to the diffusive mode as well: that a seemingly stable stratification may actually be unstable.

This revelation spurred laboratory experiments dealing with the heating of salt stratified fluids and similar sugar-salt[1] systems. Based on these experiments and dimensional arguments, it was suggested that the properties of the staircases formed would depend only on differences between the properties of the convective regions – specifically the ratio of neighbouring temperature and salinity differences, ΔT and ΔS, between these convective regions (Turner, 1965). This implies that one of the main non-dimensional governing parameters for this system should be the density ratio, which for the diffusive mode is defined as

$$R_\rho \equiv \frac{\beta \Delta S}{\alpha \Delta T} \tag{1.1}$$

where α ($\equiv -\frac{1}{\rho_0}\frac{\partial \rho}{\partial T}$) and β ($\equiv \frac{1}{\rho_0}\frac{\partial \rho}{\partial S}$) are the thermal expansion and haline contraction coefficients assuming some reference density, ρ_0. This ratio can be interpreted as a comparison between the stabilizing effects of the salinity differences and destabilizing effects of the temperature differences between steps on the the overall stratification, such that the system is more stable for high values of R_ρ and convectively unstable for $R_\rho \leqslant 1$.

Aside from the density ratio, the other non-dimensional numbers that are thought to govern this system include: the Prandtl number, $Pr \equiv \nu/k_T$, where ν is the kinematic viscosity and k_T is the thermal diffusivity; the salinity Lewis number, $\tau \equiv k_T/k_S$, where k_S is the diffusivity of salt; and (once staircases form with convection within the layers) the Rayleigh number,

$$Ra \equiv (\frac{g\alpha}{k_T \nu})\Delta T H^3 \tag{1.2}$$

where H is the layer thickness/height and g is the acceleration due to gravity.

Laboratory experiments have shown that in a stable salt-stratified system, heating from the bottom results in the formation of a (time-dependent) bottom convecting layer, followed by the formation of more layers above over time (Turner, 1968). This occurs because the buoyancy instabilities generated by the heating of the bottom are constrained to a maximum height by the stabilizing effects of the salinity gradient, and so create the first convective layer. Just above this convective layer, a high gradient region is created where the only transport processes are due to molecular diffusion

[1] Due to the difficulty of perfectly isolating heat diffusion though side walls in physical experiments, the salt-heat system is at times replaced by the sugar-salt system. The replacement is not perfect, since the diffusivities of the sugar-salt system differ by a factor of 3 while those of the salt-heat system differ by a factor of 100, but still serves to exemplify the characteristics of double diffusive processes.

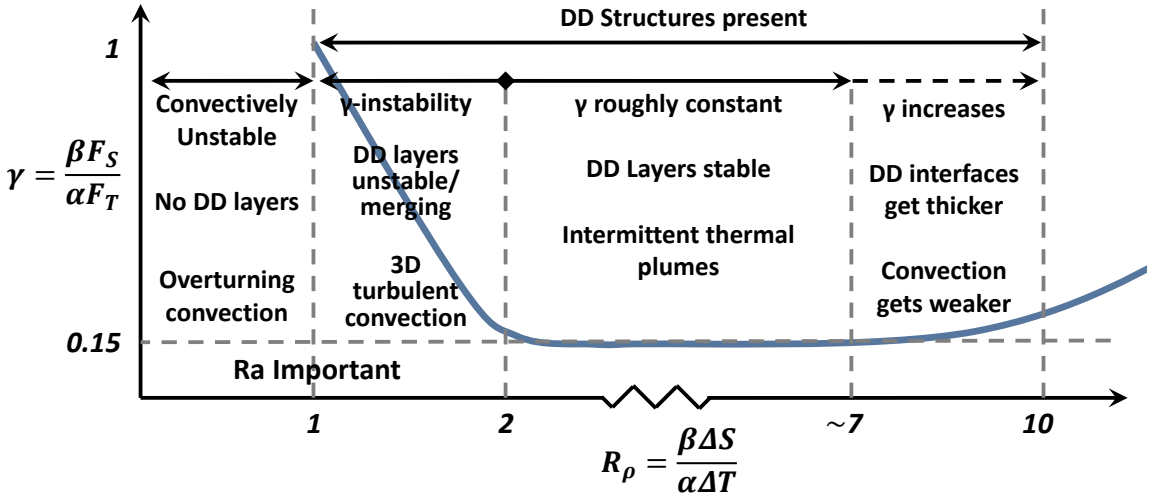

Figure 1.2: A schematic of the functional form of the density flux ratio, γ, as a function of the density ratio, R_ρ, with the characteristics of each regime shown.

– this is the diffusive interface. Since heat diffuses quicker than salt, buoyancy instabilities are generated at the upper boundary of this diffusive interface, and so begin the development of the next convective layer.

Interest in the transport properties through the diffusive interface led to more laboratory studies focusing specifically on a two layer system with a diffusive interface, heated from below and, at times, cooled from above. It was shown that the interface has a thickness that depends on R_ρ, and has a tendency to migrate vertically, with the migration rate increasing as R_ρ approaches 1 from higher values (Marmorino and Caldwell, 1976). It was also found that the transport in the convective regions is dominated by mechanical mixing for $1 < R_\rho \leqslant 2$, and by interface-dependent double diffusive convection for $R_\rho > 2$ (Crapper, 1975).

Since the heating in these experiments could be controlled, the total vertical heat flux[2], F_T (in units of $^\circ C \times m/s$), through the interface was determined and found to decrease with increasing R_ρ (Turner, 1965). An important parameter that appears in this analysis is the density flux ratio, defined as

$$\gamma \equiv \frac{\beta F_S}{\alpha F_T} \tag{1.3}$$

where F_S is the salt flux (in units of $g/kg \times m/s$), and indicates the ratio between the (non-dimensional) stabilizing flux due to salinity and the destabilizing flux due to temperature. Alternatively, the density flux ratio can be interpreted to indicate the contribution of the potential energy released from the temperature field which goes into moving the salt. It was shown by Turner (1965) that the density flux ratio is nearly constant at $\gamma \approx 0.15$ for $2 \leqslant R_\rho < 7$, and increases towards a value of 1 when R_ρ approaches 1 from higher values (Figure 1.2). This was extended by Newell (1984), who showed

[2]The parametrization of double diffusive fluxes has been an active ongoing endeavor, but as the present work does not rely on such parameterizations the reader is referred to Kelley et al. (2003) for a historic perspective on their development.

that $\gamma \approx 0.15$ up until $R_\rho \approx 10$, after which it begins to increase again. As R_ρ increases above this value, γ tends towards R_ρ/τ for a diffusion-governed background since the fluxes would depend only on the molecular diffusivities (Newell, 1984), or towards R_ρ for a background dominated by turbulence since the fluxes would be dominated by eddy diffusivity (Radko, 2015). In this high R_ρ limit, erosion of the diffusive interface becomes significant – that is, the thickness of the diffusive interface increases while the slope of the gradient decreases.

During observations of two dimensional effects on layer formation in sugar-salt experiments, it was found that sloped walls and local sources of anomalies set up horizontal gradients, which led to horizontal layer formation (Turner and Chen, 1974). The layers propagated from the sloped walls/anomaly sources until they filled the domain, and then proceeded to merge until they became stable and the merging process ended. Once stabilized, the layers were found to tilt slightly, with a large-scale circulation occurring along the top and bottom diffusive interfaces. The horizontal fluxes of temperature and salinity within the layers were observed to be slightly unbalanced, resulting in a horizontal density gradient along the tilted layers.

After the initial laboratory experiments during the birth of the field, focus shifted to numerical simulations and field observations. Much later work on the laboratory salt-heat system by Lavery and Ross (2007) showed that the diffusive interfaces were subjected to interface waves, with thermal plumes observed emerging from them. Furthermore, Lavery and Ross (2007) showed that the interfaces had a tendency to get thicker for increasing R_ρ, supporting the earlier results of Marmorino and Caldwell (1976). A later study by Ross and Lavery (2009) using acoustic measurements of the salt-heat system indicated that layer migration and merger were prominent, and that convection is driven by the thermal plumes (which are dependent upon the applied heat flux) released from the diffusive interface.

Turner (1968), Marmorino and Caldwell (1976), and Newell (1984) all observed oscillations in the temperature records near the diffusive interface, with the amplitude of the temperature oscillations decreasing with increasing R_ρ (Newell, 1984). These oscillations occured on time scales of a factor of 1 (Marmorino and Caldwell, 1976) to ~ 10 (Turner, 1968) times the buoyancy period, N^{-1}, where the buoyancy frequency, N, is defined as

$$N \equiv \sqrt{\frac{-g}{\rho_0}\frac{d\rho}{dz}} = \sqrt{g(\alpha dT/dz - \beta dS/dz)} \tag{1.4}$$

These oscillations were interpreted to be the same plume features observed later by Lavery and Ross (2007) and Ross and Lavery (2009). Turner (1968) specifically noted that the oscillations were intermittent and occurred prior to the system transitioning into the convective mode during the development of the second convective layer.

1.3 Field Observations

The layer-based definition for the density ratio R_ρ (Equation 1.1) is better suited for laboratory studies rather than for field observations due to the explicit use of the temperature and salinity differences between layers. Instead, for field observations, the definition of

$$R_{\rho z} \equiv \frac{\beta \partial S/\partial z}{\alpha \partial T/\partial z} \tag{1.5}$$

is more convenient. This definition is equivalent to Equation 1.1 if the temperature and salinity profiles are first smoothed over the steps prior to any calculation of gradients, which is the standard approach. In this context, $R_{\rho z}$ can be interpreted as the ratio between the stabilizing effects of the background salinity gradient and destabilizing effects of the background temperature gradient on the overall stratification. It is typically in the range of $1 - 10$ in field observations where double diffusive processes occur.

One of the earliest field observations of double diffusive structures was performed by Hoare (1968) in Lake Vanda, Antarctic. Several double diffusive layers were observed to exist over the course of nearly a year. The layers spanned a horizontal distance of 4 km, and showed temporal variability in their temperatures, thicknesses, and depths.

Afterwards, many observations of double diffusive staircases came from the Arctic Ocean: Padman and Dillon (1987), Timmermans et al. (2008), Zhou and Lu (2013), Zhou et al. (2014), and Carmack et al. (2012) observed the structures in the Canada Basin; Sirevaag and Fer (2012) in the Amundsen Basin; and Polyakov et al. (2012) in the Laptev Sea. Data were typically obtained by means of (ship-based or moored) conductivity-temperature-depth (CTD) profilers or microstructure profilers.

Within the Canada Basin, the staircase structures were observed to be persistent over two decades (Carmack et al., 2012) and horizontally coherent over 800 km, breaking only at the boundaries (Timmermans et al., 2008). It was shown that the bottom-most convective layer was caused by geothermal forcing (Zhou et al., 2014), and that the entire structure acts as a thermal barrier to this forcing (Zhou and Lu, 2013). Interestingly, no horizontal coherence was observed in layers seen in the neighbouring Amundsen Basin (Sirevaag and Fer, 2012).

The steps within the Arctic staircase structure were found to be non-uniform in height, possibly implying non-uniform fluxes through the staircase structure (Padman and Dillon, 1987). It was further suggested that the convective structure within layers changed from intermittent buoyant plumes to convection cells as $R_{\rho z}$ approaches 1 from higher values (Padman and Dillon, 1987), similar to those seen in the buoyant convection of single component fluids. These suggestions were supported by the observation that the steps are in a mild state of turbulence, with signals of intermittent small-scale flow structures within the convective regions of the steps, impinging upon the diffusive interfaces (Zhou and Lu, 2013).

In the Laptev Sea, Polyakov et al. (2012) observed that the staircase structure was also visible in vertical profiles of horizontal currents, and that the shear produced by these structures was not

enough to overcome the effects of buoyancy in the diffusive interfaces. Furthermore, it was shown that the layers were getting warmer, saltier, and lighter with time, and that their properties were unaffected by passing eddies.

Apart from the Arctic and Antarctic regions, double diffusive structures have also been observed in several lakes around the world. The most prominent and persistent examples include: Lake Nyos in Cameroon (Schmid et al., 2004), Lake Kivu on the border of Rwanda and the Democratic Republic of Congo (Schmid et al., 2010; Sommer et al., 2013), and Powell Lake in Canada (Scheifele et al., 2014). The structures are also seen more intermittently in other lakes, appearing and disappearing with changes in the seasonal stratification (von Rohden et al., 2010).

Within these lakes, it was observed that the structures develop from and are maintained by external sources such as large surface cooling events (Schmid et al., 2004) or geothermal bottom heating (Scheifele et al., 2014). In the former case, it was observed that the staircase structure formed over the period of 9 months after the cooling event; in the latter, staircase formation may be the result of hundreds or thousands of years of weak heating. The layers were observed to be horizontally coherent for scales on the order of many kilometers (Schmid et al., 2010; Scheifele et al., 2014), but may be disturbed by horizontal intrusions (Schmid et al., 2010).

A closer inspection of the diffusive steps revealed that the temperature interfaces were thicker than salinity interfaces (Sommer et al., 2013), and that the layers are in a state of active convection (Schmid et al., 2010). It was further observed by Scheifele et al. (2014) that for $R_{\rho z} \lesssim 3$ the system began to exhibit a dependence on the Rayleigh number, which is indicative of a regime similar to that of single component buoyant convection. These observations reinforce the idea of intermittent buoyancy driven convective instabilities arising from the diffusive interface, with a transition to turbulent convection for low density ratios.

1.4 Numerical Modelling

At the same time that double diffusive convection was being studied in laboratory and field settings, numerous analytic expressions and numerical models were developed to investigate the behaviour of the diffusive interface and resulting staircase structure. A one-dimensional numerical model was created by Shirtcliffe (1969) in order to simulate a stable salt-stratified gradient heated from below. In the model, the molecular diffusivity was replaced by an eddy diffusivity in buoyantly unstable regions to mimic the effects of convective eddies. This model successfully reproduced the formation and evolution of the bottom convecting layer – as well as the development of the following layers – from initially linear gradients, and suggested that the schematic of convecting regions separated by diffusive interfaces was a correct interpretation of the staircase structure. A similar one-dimensional model was described more recently by Toffolon et al. (2015), and (with tuning) was used to reproduce the staircase structure in Lake Kivi, Lake Nyos, and Powell Lake.

Linear stability analysis and direct numerical simulation (DNS) of the development of double diffusive instabilities from initially linear gradients by Noguchi and Niino (2010a) showed that the instabilities begin as exponentially growing vertical oscillations, consistent with linear theory, and

develop into overturning convection. After attaining some critical R_ρ, the instability field spontaneously develops into layers which grow slowly in thickness, and merge over time. Noguchi and Niino (2010b) further showed that the layer mergers occur in two forms: one where the diffusive interface erodes, and the second where a convective layer erodes. These mergers were shown to be the result of vertically asymmetric turbulent entrainment from adjacent layers.

Although examined primarily with interest in the astrophysical case[3], Rosenblum et al. (2011) showed again that the initial exponential growth of instabilities is consistent with linear theory. Furthermore, they also showed that the formation of the staircase structure is consistent with a proposed mechanism responsible for layer formation in the salt finger mode – the γ instability (Radko, 2003).

In a linear stability analysis of perturbations to a linear gradient system by Radko (2003), it was found that the growth rate eigenvalues of the characteristic equation have a positive real root – implying exponential growth – only when γ is a decreasing function of R_ρ. This γ instability implies that vertical differences in γ will grow in this regime, and result in vertical convergences and divergences of salt and heat, which lead to the formation of layers. As this only occurs in the region for which γ is a decreasing function of R_ρ, for the diffusive mode this would imply that layer growth (and merging) is only possible for $R_\rho < 2$.

The stability of an established diffusive interface was studied by Huppert (1971), who showed that the interfaces within the staircase structure were unstable for $R_\rho < 2$, resulting in layers merging consistently until reaching a stable state. It was noted that this was a local criterion only, and that merging may continue in other regions even if one section is stable.

A study performed by Linden and Shirtcliffe (1978) of the double boundary (one for temperature, one for salinity) structure of an individual diffusive interface showed that the convection is intermittent and reminiscent of the convective instabilities that occur in the fingering mode (Stern, 1969). Their model of the interface worked best for $3 \leqslant R_\rho \leqslant 7$; at larger R_ρ the convection was too weak to remove the buildup of temperature and salinity at the interface, whereas below this range interface entrainment from the convective regions became important and increased the fluxes. It was later shown by Flanagan et al. (2013) that 3D effects (which are an indicator of turbulent convection) only become prominent for $R_\rho \leqslant 2$. This reinforces the idea that convection gets stronger in the layers as R_ρ approaches 1, from higher values.

Further work by Carpenter et al. (2012) on the linear stability and direct numerical simulation (DNS) of a single diffusive interface indicated that the instabilities develop in the boundary layers of the interface, as opposed to within the interface core. Furthermore, the instabilities were found to be of the purely convective type, and are therefore time-dependent.

[3]Although presented here as an oceanographic phenomenon, double diffusive convection is found in many other fields where compositional gradients that oppose one another are found. Some examples include structure and evolution of stars and planets in an astrophysical context (e.g. Nettelmann et al. (2015)) and multi component alloy solidification in metallurgy (e.g.Beckermann and Viskanta (1989)).

1.5 Research Focus

To date, the work done in the field, laboratory, and numerical studies of the diffusive layering mode of double diffusive convection is consistent with the common explanation for the mechanisms involved in the process. The use of the density ratio, R_ρ, as the main governing parameter has become standard, along with the $1 < R_\rho < 10$ range for the identification of where double diffusive processes can occur (Figure 1.2).

Spontaneously emerging staircase structures are ubiquitous, and used as a main identifier for the occurrence of double diffusive convection. The explanation that the staircase structure is a product of vertically stacked convective layers inter-spaced by molecular-diffusion governed interfaces is strongly supported. Layers have been observed to form and merge, and thus be unstable, for $R_\rho \leqslant 2$, but stable for $R_\rho > 2$. Layer merging is most likely explained by differences in the convective entrainment between adjacent layers.

The formation mechanism of these structures is still contested, but likely caused by vertical deviations in the amount of energy transfered from the destabilizing temperature gradient into the convective motions, which rearrange the stabilizing salinity gradient. This energy transfer is encompassed in the density flux ratio, γ. It is observed that γ is a decreasing function of R_ρ for $R_\rho \leqslant 2$, is near constant for $2 < R_\rho \leqslant 10$, and an increasing function of R_ρ for $R_\rho > 10$.

Numerical studies have indicated that as R_ρ approaches 1 (from higher values) the convective regime within the layers changes from intermittent buoyant plumes to fully three-dimensional turbulent convection, where the governing parameter switches from R_ρ to Ra; the transition region between the two regimes occurs at $R_\rho \approx 2$. The plumes are formed in the thermal boundary layer of the interface and so depend on its existence.

An important aspect of this field of study is the proper modelling of the transport properties through these double-diffusive structures, and although much work has been done in studying the mechanisms involved in double diffusive convection, a more complete understanding of the physical processes involved is still desired. In this respect, the numerical and laboratory studies of double diffusive convection are far more advanced than observational studies, and much work needs to be done to bring the observational results to the level of the other two approaches.

This lag in field observations exists primarily because of restrictions in sampling procedures, such that vertical temperature and salinity profiles are attained either at multiple locations around the same time, or at one location over time. In both cases only two dimensions of the staircase structure and evolution are covered. Furthermore, due to the inherent noise in natural environments, it has been difficult to precisely detect what is occurring within the layered structure in these environments.

Due to this need for reconciliation between field studies and numerical/laboratory studies, the aim of the present work is to further observe and describe both the spatial structure and temporal evolution of the double diffusive staircase structure in a natural environment. The main goal is to characterize the dynamics of both the overall staircase structure, as well as the features within the individual layers that make up that structure.

The dynamics of the entire staircase structure should help elucidate possible formation and maintenance mechanisms of these large scale structures, which can then be compared to the mechanisms for staircase formation proposed by laboratory and numerical studies. Any variability of the structure of the layers could help identify possible factors which contribute to the large scale properties of these structures. Comparison of the observed variability of the layers with the layers obtained from numerical studies would help validate the assumptions behind those studies, specifically whether or not a one dimensional approach is appropriate in modelling the double diffusive system.

Study of the variability within the layers could help identify the convective regime within the layers, which is imperative to properly understanding and modelling the fluxes through these structures. A more complete understanding of the convective regime within the layers would ultimately assist in creating better parameterizations of the fluxes through double diffusive structures, which could be used to better model the transport of heat and salt throughout the ocean.

Chapter 2

Research Site and Methods

The intention of this work is to describe the spatial and temporal properties of double diffusive (DD) staircase structures in the diffusive regime, as seen in the relatively stable environment of Powell Lake, British Columbia. To properly describe the dynamics of these structures, observations were made of the structure and temporal evolution of both the individual steps, on the scales of centimetres and minutes, as well as the entire staircase structure, on the scales of kilometres and years.

The structure and dynamics of the overall staircase structure were studied using a data set obtained from four annual research trips, consisting of centimetre-scale (in the vertical) conductivity-temperature-depth (CTD) profiles at various locations along the length of the south basin of the lake. The dynamics of an individual step within this structure were studied using a data set obtained from a month-long mooring deployment consisting of thirty eight temperature probes and two current meters.

2.1 Powell Lake, British Columbia

Powell Lake is located near the city of Powell River, BC, approximately 170 km north-west of Vancouver along the Sunshine Coast (Figure 2.1). It is a meromictic lake that was once a fjord connected to the Strait of Georgia. However, roughly 11,000 years ago, it was landlocked due to post-glacial isostatic rebound after the last ice age. After this event, its southern sill rose, and hence the lake surface is now roughly 50 m above sea level (Mathews et al., 1970).

The lake is roughly 50 km long and 2 km wide, with six basins connected by shallower sills, first observed in a bathymetry study conducted by Mathews (1962). The lake has steep sides with a flat bottom – common to ex-fjords – and reaches a maximum depth of around 350 m in the southern basin. Williams et al. (1961) found that the two southernmost basins contain warmer, trapped relic sea water, which is transported vertically primarily by molecular diffusion (Sanderson et al., 1986). The other four, northern basins are relatively fresh. This is likely because most of the fresh water input is into those basins, where turbidity currents can flush the basin floors during sedimentary discharge (Sanderson et al., 1986).

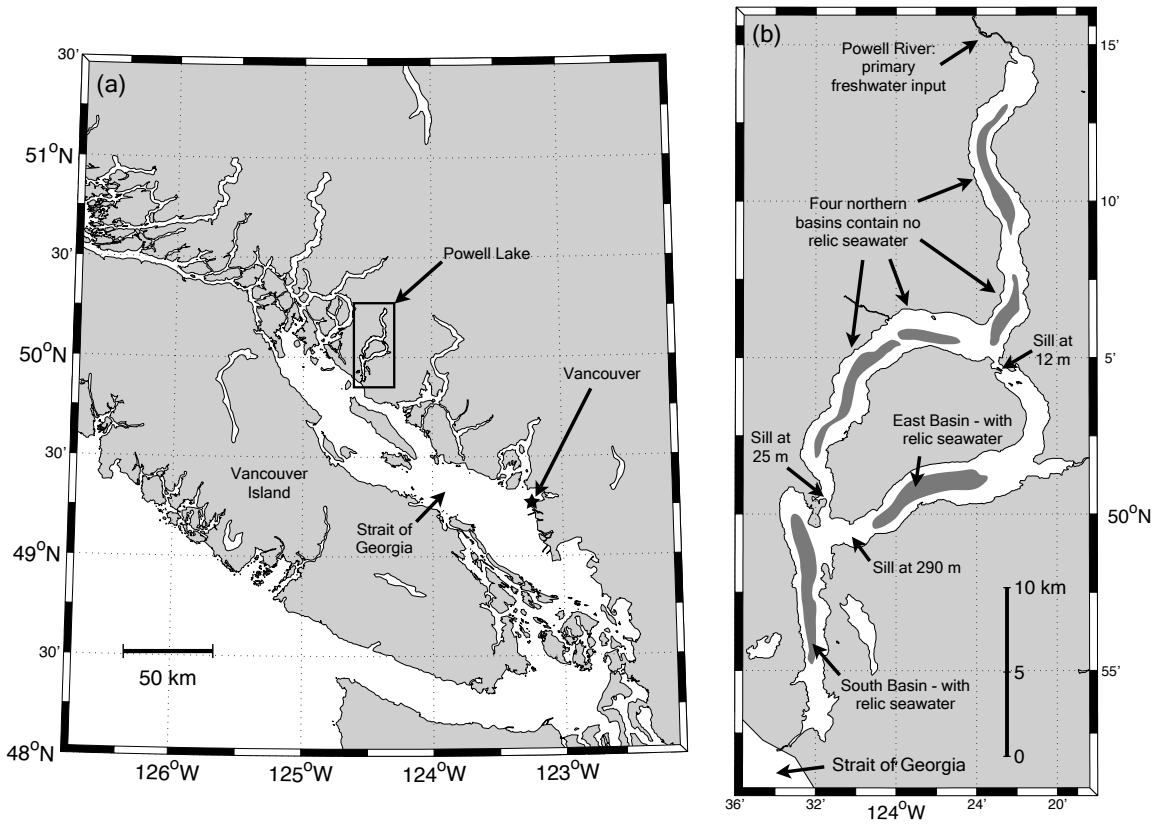

Figure 2.1: a) The location of Powell Lake, in Powell River, BC. **b)** The multiple basins of Powell Lake; the South Basin being the location of study. Adapted from Scheifele et al. (2014). ©American Meteorological Society. Used with permission.

The lake bottom of the southern-most basin is composed of a methane and pyrite rich "gelatinous ooze" (Sanderson et al., 1986), with the trapped relic sea water near the bottom containing high levels of hydrogen sulphide, pyrite, and iron sulphide (Perry and Pedersen, 1993). The near-surface freshwater exits into the Strait of Georgia via a man-made dam on the south side of the southern basin, which raised the lake level by a few metres when it was completed in 1912.

The presence of warm salty water near the bottom suggests a high susceptibility to double diffusive instabilities. A micro-structure study performed by Osborn (1973) showed irregular temperature gradient variations near the lake bottom. By means of analyzing sediment core samples, Hyndman (1976) found that the geothermal heat flux was 27 ± 11 mW/m^2 at the lake bottom.

A more recent study dealing specifically with the DD properties of the lake was conducted by Scheifele et al. (2014). Their study showed that there were several vertical regions below 250 m, where staircases indicating DD instability could be found (Figure 2.2a). Their work focused on characterizing the statistical properties of the DD steps found in the relic salt water region below a depth of 325 m, which exhibited the most coherent DD structures.

The DD steps were found to have a mean mixed layer height of 70 cm, a mean diffusive interface height of 20 cm, and mean differences between steps of 4 m°C in temperature and 2 mg/kg in

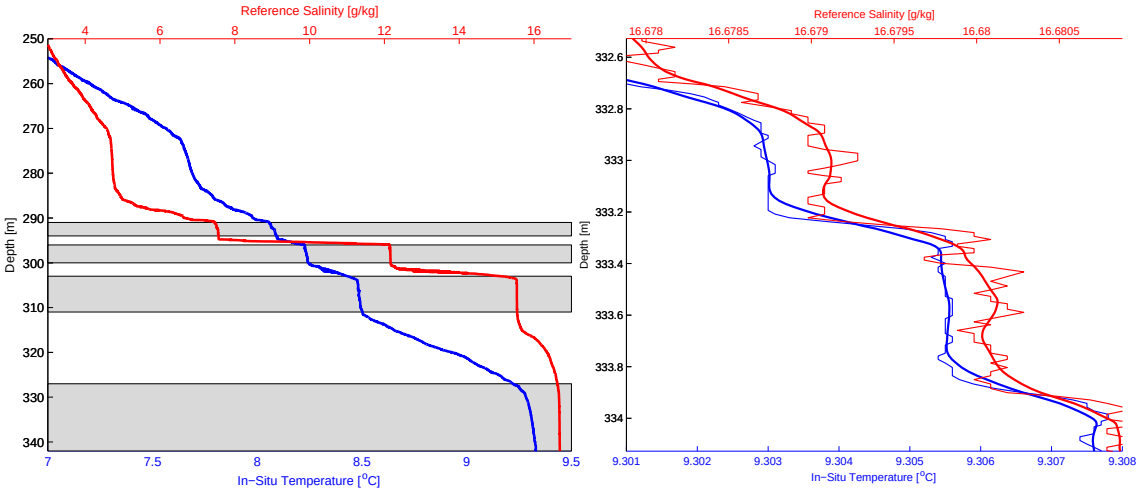

Figure 2.2: a) In-situ temperature and Reference Salinity profiles of the salt water layer in the southern basin of Powell Lake. DD active regions are shaded in gray. **b)** Close-up of a few DD steps in the lowest DD active region, near the lake bottom; raw data shown in thin lines and smoothed profiles in which electronic noise is filtered out in bold.

salinity[1]. Furthermore, consistent estimates of the heat flux though interfaces in the staircase structure and in the linear temperature gradient region at 320 m were found to be in agreement with the value previously found by Hyndman (1976) in the bottom sediments. Following the observations of Scheifele et al. (2014), the focus of the present work is again only on this lowest DD active region, below a depth of 325 m.

2.2 Annual CTD Profiling Surveys

Beginning in 2012, an annual survey using a CTD profiler was carried out in order to observe the dynamics of the overall staircase structure in the southern basin of Powell Lake. The survey involved taking a number of vertical CTD profiles along the length of the lake[2] during each sampling trip (Figure 2.3). The CTD data obtained over the four years included: 21 profiles from July 2012, capturing the middle and northern sections of the lake; 18 profiles from June 2013, capturing the southern and central sections; 11 profiles from May 2014, capturing the southern and central sections; and 7 profiles from June 2015, capturing the entire lake but at a larger profile spacing.

Of the 57 CTD profiles obtained in the four annual surveys, only 49 were used in the identification of the DD steps and layers[3]. This was because 4 profiles from the 2013 survey, 2 profiles from the 2014 survey, and 2 profiles from the 2015 survey reached bottom before entering the bottom DD active region. These profiles were in the southern part of the lake.

[1] All salinity values stated are on the TEOS-10 Reference-Composition Salinity Scale with no salinity anomaly (IOC et al., 2010).

[2] The term 'lake' will be implied to refer to the southern basin of Powell Lake only.

[3] Any further use of the terms 'steps' and 'layers' will be understood to refer to DD steps and DD layers.

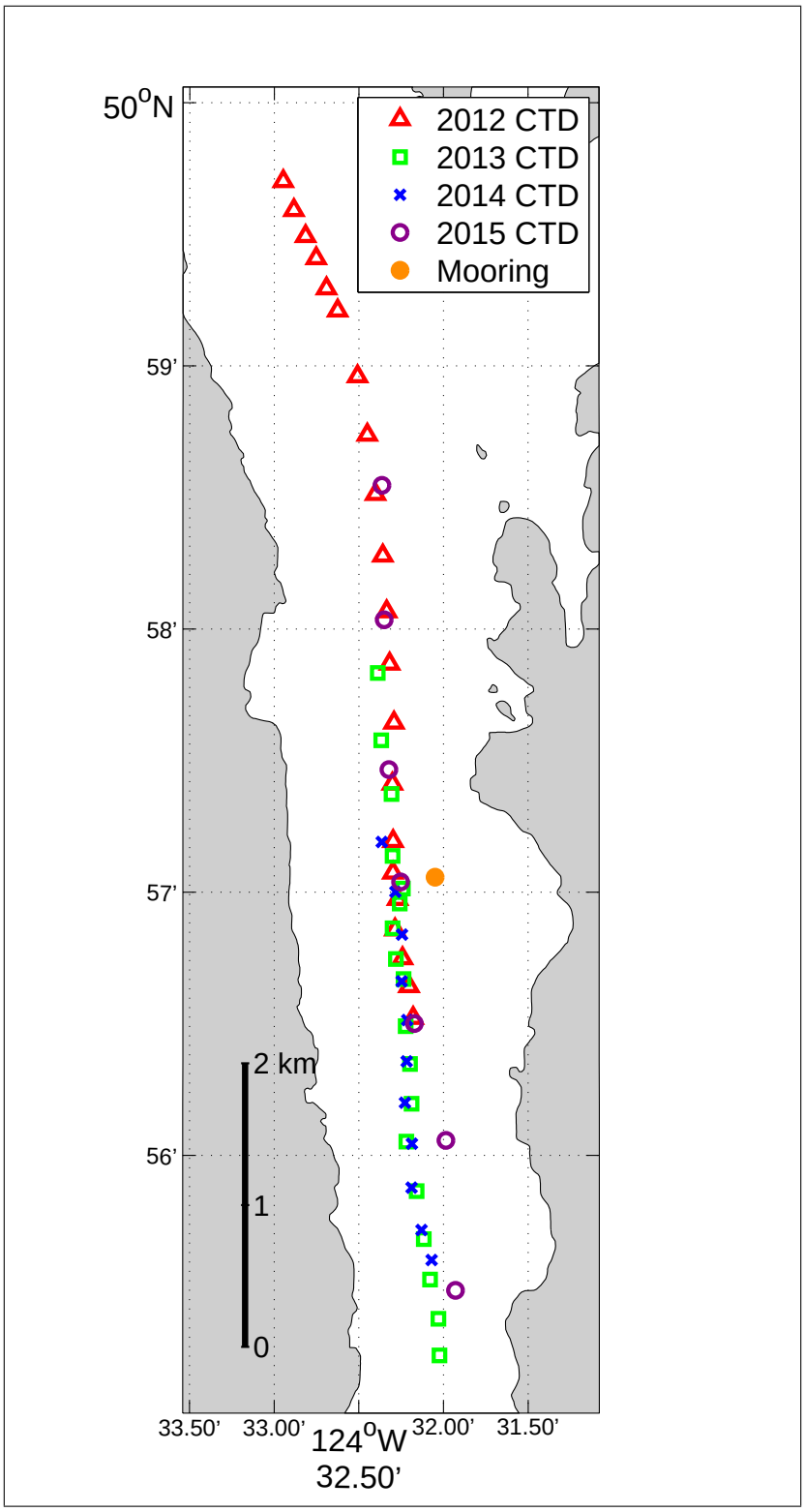

Figure 2.3: The locations of the CTD profiles taken during the 2012 - 2015 CTD surveys, and the October 2014 mooring.

The CTD profiler used for these surveys was a Sea Bird SBE 25[4], which was set to its maximum sampling rate of 8 Hz. In order to resolve the length scales of the DD steps (typically less than 1 m), the lowering rate of the profiler was chosen to be 10 cm/s in the salt water region (depths below 250 m) and 1 m/s above this region. This procedure was arranged in order to save time, but even so, each cast took around 45 minutes to complete. The combination of the 8 Hz sampling rate and 10 cm/s drop rate resulted in a vertical resolution of $\sim$1.5 cm.

The response time of the CTD temperature sensor is 0.1 s, whereas the conductivity sensor's time response is best described by the quotient of the sensor volume and the pump flow rate: 2.4 mL $\div$ 15 mL/s $\approx$ 0.16 s (Scheifele, 2013). At a lowering rate of 10 cm/s, these responses produce a spatial resolution of 1 cm and 1.6 cm in the temperature and salinity time series, respectively. These resolutions correspond to the smoothing effects that the sensors produce in response to instantaneous changes in temperature and salinity; they were not corrected for in subsequent processing since they were of the same order as the resolution due to the lowering rate and sampling frequency. The two sensors were connected in series, so that the conductivity sensor would sample a parcel of water 0.2 s later than the temperature sensor. This temporal offset between sensors was corrected for by applying a 0.2 s time shift to the conductivity data during preprocessing.

The temperature and salinity resolutions of the time series were 0.1 m$^\circ$C and 0.1 mg/kg, and the electronic noise in the signals was estimated to be $\pm$ 0.2 m$^\circ$C and $\pm$ 0.1 mg/kg, respectively. This noise can be seen as the variability in the raw data of Figure 2.2b in the region between 333.4 m and 333.8 m.

The manufacturer's quote for the temperature sensor's maximum calibration drift rate is 2 m$^\circ$C/yr, but no deviations were evident in the data or independent calibrations and thus no corrections were made over the 4 year series. Conductivity measurements did change from year to year, and intermittent calibrations were not accurate enough to fully remove these drifts. Instead, the data were manually adjusted so that waters of the same temperature had the same salinity; the 2013 survey salinity data was adjusted by +8.4mg/kg, the 2014 data by +5.5mg/kg, and the 2015 data by +22.1mg/kg.

Since the CTD profiler was connected to the boat winch via a cable, any boat motions were transferred to the movement of the CTD profiler, which could introduce variability into the temperature and salinity data. This variability would appear similar to the noise in the sensors but would be more intermittent. In order to minimize this movement-related noise the sampling was performed between sunset and sunrise, when the wind and waves were most calm. A 'lander' cage was attached to the CTD profiler bottom in order to prevent sediments from fouling the sensors, and to also allow the CTD profiler to sample to a constant 0.5 m from the bottom during each cast.

The CTD pressure variable was converted to a depth via a correction factor obtained from the comparison of the boat winch 'wire out' reading at the bottom of the casts and the bottom pressure reading from the CTD; this conversion factor was 1.0137 m/dbar. To compare the profiles obtained from various years, the depth data was corrected for the varying lake surface heights using a data

[4]See http://www.seabird.com/sbe25-sealogger-ctd.

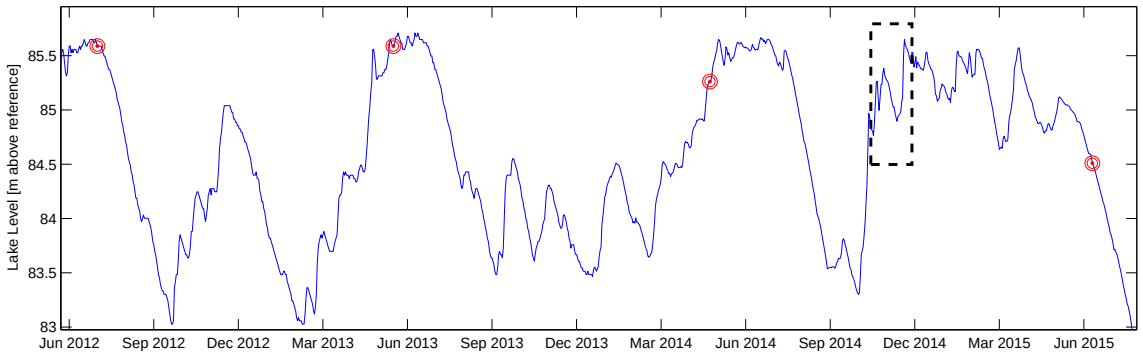

Figure 2.4: Powell Lake heights above their reference level, obtained by Brookfield Renewable Power at the site of the dam. CTD survey dates shown as circled red points, and mooring duration indicated by dashed box.

set provided by Brookfield Renewable Power (Figure 2.4).

In order to save time, only depths between 250 m and the bottom were measured with the profiler, and it was kept at a depth of 250 m while the boat was maneuvered to the next sampling location. This 'tow-yoing' method became inefficient for sampling station spacings greater than 500 m, and was not possible when more accompanying sensors were attached to the CTD, which had the effect of draining the memory and battery life at a quicker rate. In these situations (which occurred mainly during the 2015 survey), the CTD profiler would be brought back up to the surface after each cast, so that the batteries could be replaced and data downloaded as necessary.

2.3 Temperature Sensor and Current Meter Mooring

A mooring was deployed in the central section of the lake from late October to early December 2014 (Figure 2.3, Figure 2.4). The mooring was instrumented with 38 temperature sensors and 2 current meters (Figure 2.5). The temperature sensors used on the mooring were the SeaBird SBE 56[5], RBR Solo [6], and RBR TR1050[7]; the current meters used were InterOcean Systems Inc. S4A Current Meters[8]. Upon retrieval, it was discovered that one of the 38 temperature sensors used on the mooring had stopped functioning due to a leak from a faulty O-ring. All other components were functioning properly upon retrieval.

Thirty-six of the temperature sensors were attached to a rigid plastic beam in a 2 metre vertical line array with 18 of the sensors spaced 7 cm apart in the top of this section and 18 sensors spaced at 3.5 cm apart on the bottom. This spacing was chosen after examining results from a previous mooring deployment in Powell Lake by Scheifele (2013) in which sensors were spaced 14 cm apart. The other two temperature sensors were positioned such that one was placed on the acoustic release 1 metre from the mooring bottom, while the other was attached to the line 1.5 m below the

[5] See http://www.seabird.com/sbe56-temperature-logger.

[6] See http://www.rbr-global.com/products/small-single-channel-loggers/temperature-rbrsolo-t.

[7] See http://www.rbr-global.com/products/dual-channel-loggers/temperature-a-depth-rbrduo-td.

[8] See http://www.interoceansystems.com/s4specs.htm.

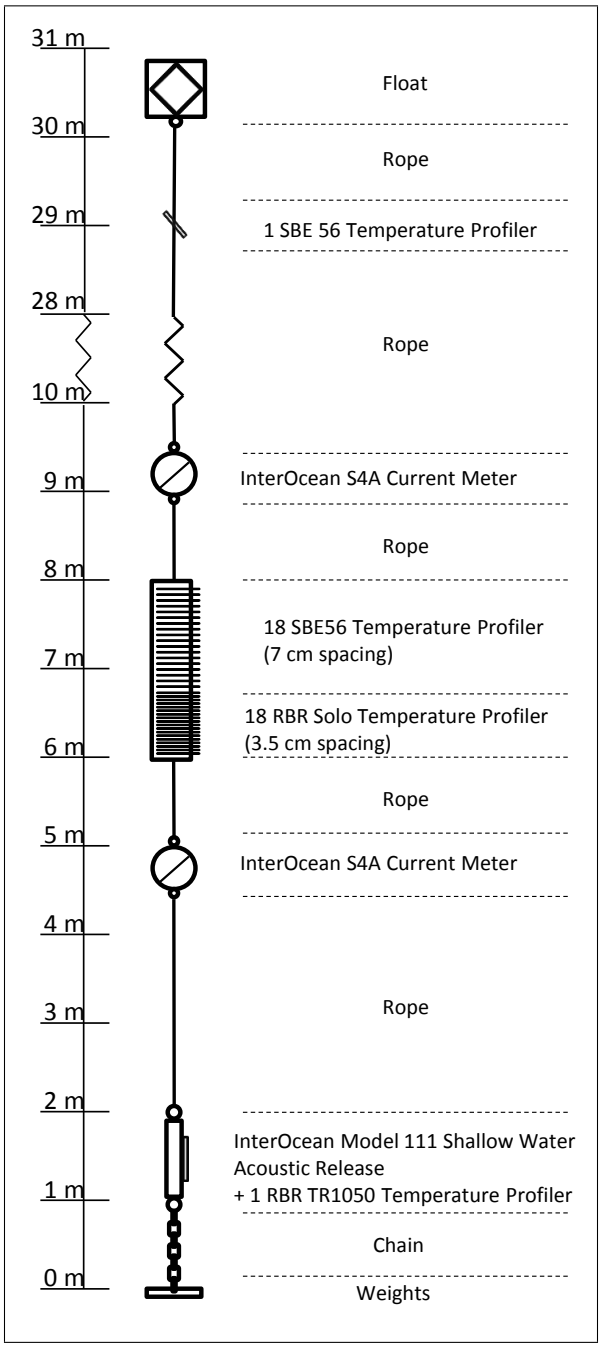

Figure 2.5: A schematic of the mooring deployed between October and December of 2014, showing the location of the 2-m vertical line array of temperature sensors with current meters above and below, and the location of the other two temperature sensors.

float, in a region with a linear temperature gradient.

The RBR Solo temperature sensors were set to a sampling rate of 2 Hz, whereas the SBE56 and RBR TR1050 temperature sensors were set to a sampling rate of 1 Hz. All sensors had a temperature resolution of 0.1 m°C, with an electronic noise level of $\pm$ 0.2 m°C. After the mooring was retrieved, the temperature sensors were all placed in a calibration tank to inter-compare their readings while bringing the temperature of the calibration bath to values found in the lake. The sensors showed offsets of up to 1 m°C from the mean reading, with a slight dependence of this offset on the temperature of the bath. The moored temperature data were corrected by removing the mean offsets for each sensor.

The two current meters were positioned one above and one below the 2 metre section of temperature sensors. These current meters function by creating an AC magnetic field and then reading the induced potential associated with the flow of salt water (a conductor) through that field, across two sets of perpendicular electrodes (Lawson et al., 1983). The magnetic field may be disturbed if there are other conductors nearby, and so the current meters were spaced 1 meter apart from the nearest temperature sensors to minimize these disturbances.

The current meters were set to record 1 minute-averaged currents once every 6 minutes, and instantaneous heading and tilt once every 30 minutes. Calibration tests were performed both before the deployment and after retrieval of the mooring. This involved testing the out-of-water heading response, and the in-water speed and direction response to oscillatory motion and rest. The calibration showed that both sensors had a heading resolution of 1° and a tilt dependent bias of $\pm\ 3^\circ$; both sensors had a speed resolution of 2 mm/s. While running on the 2 second-average setting the noise in the speed readings of the instruments was observed as a variability of $\pm$ 2 mm/s in the signal, in accordance with manufacturer specifications; however, the instrument manual indicates that for the 1 minute-average setting the noise level would be below the measurement resolution.

The tilt record on both current meters stayed fairly consistent between $0-1^\circ$, indicating that the mooring remained almost vertical and hence sampled the same depths at all times. The instrument heading also remained fairly constant except for a slow drift over the first two weeks (not shown). However, raw current speeds of the upper current meter were consistently larger than those of the lower current meter throughout the entire mooring deployment. This difference appeared to drift from about 3 cm/s to 5 cm/s over the first few weeks of deployment, and then stabilized for the remainder of the deployment (Figure 2.6, top left). Neither the strength nor the direction (not shown) of the long term trends in the currents seemed reasonable, and the drift seen in the initial weeks of the deployment also suggested some instrumental problem.

During the calibration tests done after the mooring was retrieved, the zeros on the current meters were seen to differ by up to 2 mm/s between tests where the lake residue was left uncleaned on the electrodes and after it was wiped off with alcohol. The long term drift observed in the raw currents was still far greater than this difference, and so, unlikely to be caused purely by the buildup of compounds from the lake water onto the electrode surfaces. The pre- and post-calibrations were preformed in salt water, but not with the exact composition of the waters at the bottom of Powell

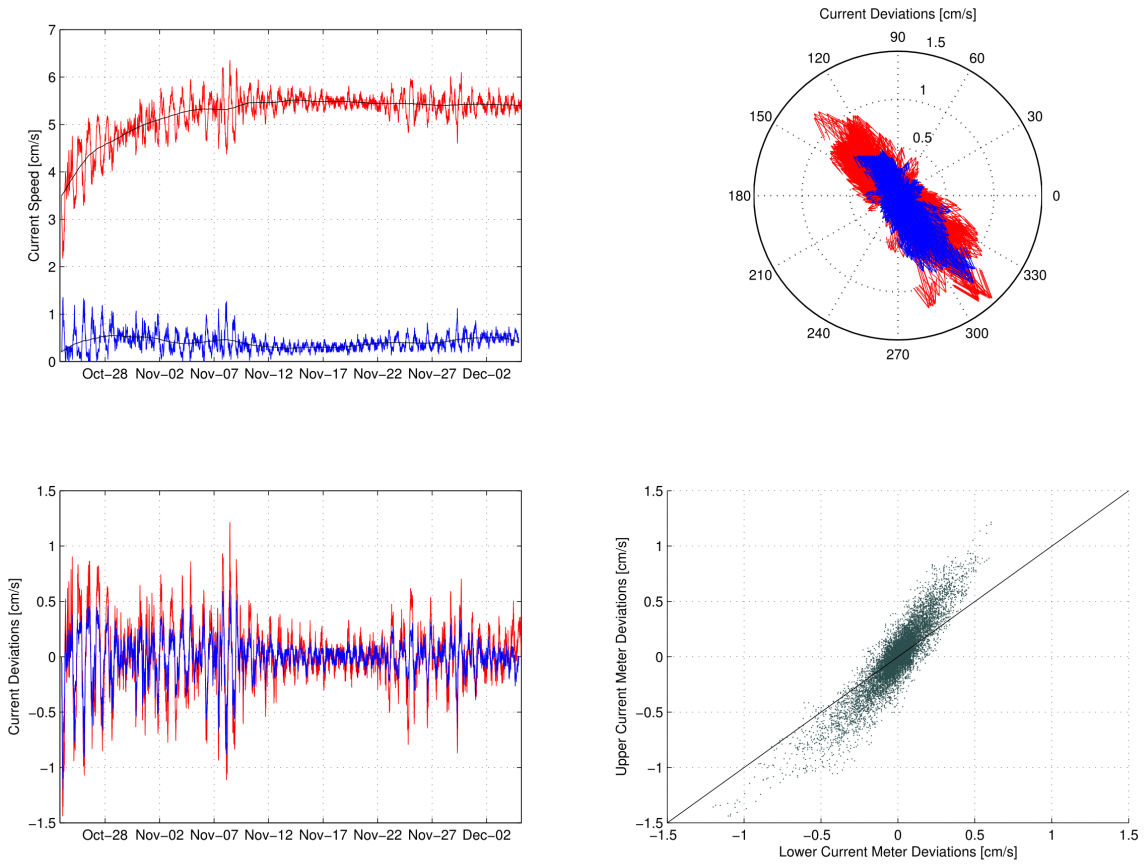

Figure 2.6: Top Left: The 18 minute mean current speeds measured by the lower (blue) and upper (red) current meters during the period of the mooring deployment, with the long term trends shown in black. **Top Right:** The deviations from the long term trends, with major axes in the 131° direction for the lower current meter and 139° for the upper current meter. (East is 0° and North is 90°) **Bottom Left:** The current deviations along the major axes over the course of the mooring deployment. **Bottom Right:** The enhanced response of the upper current meter (S4b) relative to that of the lower (S4a), shown as a slope greater than 1:1 (black line).

Lake, such that any junction potential effects between the electrodes and the anoxic deep waters of Powell Lake would not be reproduced.

An attempt was made during the 2015 CTD survey to determine whether the difference in the long term signal between the two current meters was a feature of the velocity structure within the lake or simply a sensor issue. This was done by profiling the current meters (much like the CTD profiler) so that both current meters would profile the same vertical regions within the lake at (nearly) the same time. Contamination of this data by the motions of the boat, however, made the tests inconclusive.

Although the validity of the long-term trends within the currents remains in question, it was decided that these trends should be removed and only the shorter-period deviations be considered in subsequent analysis. Note that the correlation of what seem to be advective features in the temper-

ature record with these current deviations strongly suggest that the mean currents, in this stagnant bottom water, are in fact very close to zero ($<\sim$0.5 mm/s).

The current deviations formed an elongated region of scatter, with the major axes being 131° for the lower current meter and 139° for the upper current meter– both in the northwest direction. This direction is not entirely aligned in the along-lake direction, possibly due to the interaction with the bottom topography, but shall nonetheless be referred to as the along-lake direction.

The variability in the current records were highly correlated (Figure 2.6, bottom left); however, the upper current meter consistently recorded slightly stronger variations than observed by the lower current meter (Figure 2.6, bottom right). It is unclear whether this difference is due to real vertical shear in the water column or sensor sensitivities as the currents were much smaller than the manufacturer accuracy specification ($\pm$1 cm/s). As such, all that was assumed was that the two were highly correlated.

Chapter 3

Analysis and Results

The types of data acquired for this work were varied in nature, encapsulating the wide range of length and time scales involved in DD processes and their associated staircase structure. Accordingly, the analysis of the data varied equally and was divided into three distinct approaches: the identification of the layer structure of the DD steps, and the evaluation of the horizontal coherence and temporal evolution of this structure; the identification and subdivision of the motions present within the lake which apply to the large scale DD structure and to the small scale DD step; and the identification of a single DD step and the dynamics within it.

3.1 Structure and Dynamics of DD Layers

In order to identify individual steps in the temperature and salinity profiles from the CTD data, an approach similar to that of Polyakov et al. (2012) and Scheifele et al. (2014) was employed. This required identifying the transition regions between the high-gradient diffusive interfaces, the step "treads", and the near-uniform convective regions, the step "risers".

To identify these features, the temperature and salinity profiles were first smoothed with a 15 cm running mean filter to eliminate the small-scale variability due to instrument noise. A background profile was then constructed by applying a 2 m running mean filter to the data to smooth out the features of the DD steps. The difference between the smoothed and background profiles showed peaks that correspond to the transition regions between the diffusive interfaces and the convective regions (Figure 3.1). These transition points were more evident in the temperature profiles than the salinity profiles, and thus the former were used to isolate the step risers. Only step risers which were taller than 15 cm and that contained temperature variations less than 1 m$^\circ$C in the smoothed profiles were retained, since any features with smaller vertical extents and larger temperature variations than this more closely resembled the step treads.

In order to combine the identified risers from individual profiles into spatially coherent layers, an analysis procedure was created combining two different approaches used to identify DD layers in past studies. The approach taken by Padman and Dillon (1987) and Schmid et al. (2010) was to compare a certain property of the risers from adjacent profiles; the risers whose properties were

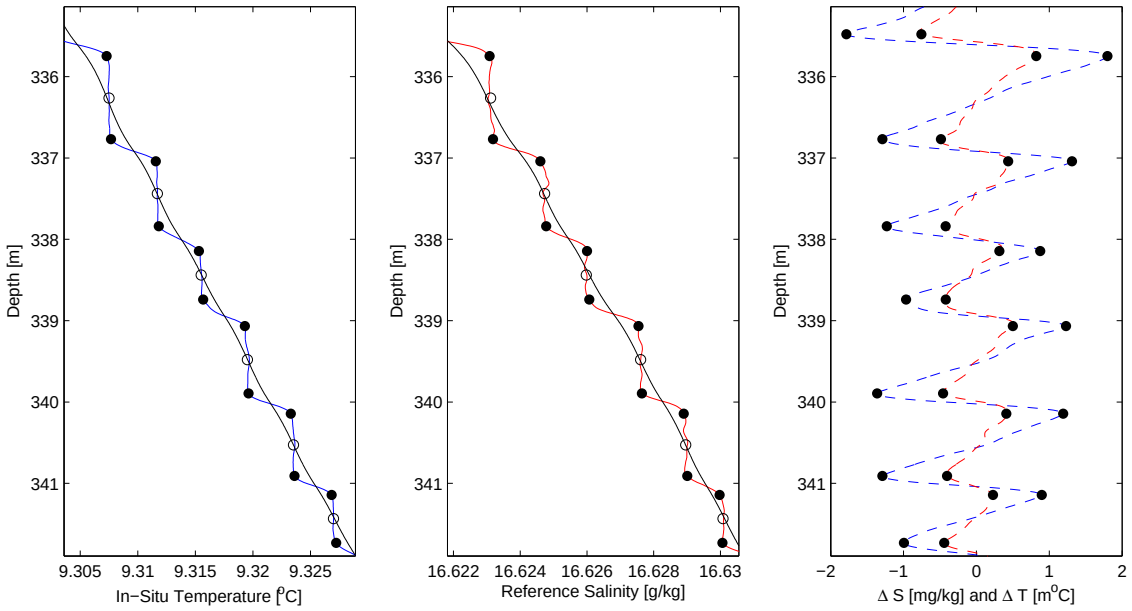

Figure 3.1: Left to right: The 15-cm running mean smoothed (blue) and 2-m running mean background (black) in-situ temperature profiles; the smoothed (red) and background (black) reference salinity profiles; and the differences between the smoothed and background temperature (dashed blue) and salinity (dashed red) profiles. Shown are typical examples for illustrative purposes only, with the transition points between convective regions and diffusive interfaces marked with filled circles and the mean riser properties shown with open circles.

closest in the adjacent profiles were combined to form a single layer. In contrast, Timmermans et al. (2008) and Scheifele (2013) suggested that individual layers would form distinct clusters on a temperature-salinity (T-S) plot, and thus could be identified by looking at all of the CTD profiles together in this way. Combining the two methods, an algorithm was created that would match risers from adjacent profiles into layers, according to a criterion that would produce clusters in a temperature-salinity plot which were most agreeable with a visual inspection. Examining the various clustering criteria options (eg. possible combinations of mean riser salinity, temperature, density, or depth) indicated that matching closest profile-to-profile mean riser salinity produced the best results.

The layer finding algorithm successfully identified around 25 layers per survey in the lowest DD active region of the lake. These layers appear as discrete clusters on T-S diagrams (Figure 3.2). The clusters appear tightest in a central region of the T-S diagram, and begin to overlap or spread out in regions further away from the center. These clusters have an elongated shape, with the slopes of the clusters not aligned along isopycnals, indicating that the density in individual layers is not constant along the lake.

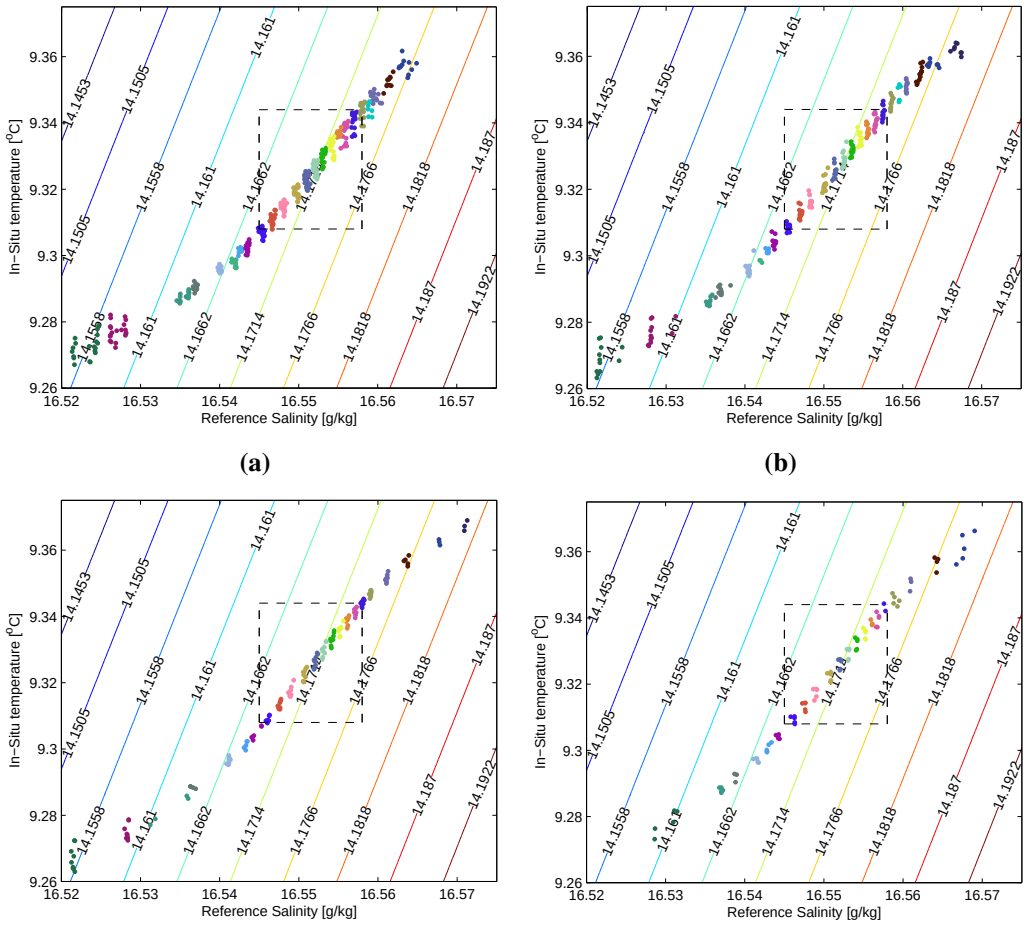

Figure 3.2: The DD layer clusters in T-S space shown with contours of potential density [kg/m^3] computed with a reference at 325 dbar. Individual layers are shown as different coloured clusters for the **a)** July 2012 data, **b)** June 2013 data, **c)** May 2014 data, and **d)** June 2015 data. Dashed box region shows the central portion of the steps with the most coherent properties.

A potentially useful characteristic of the clusters is the horizontal density gradient (Timmermans et al., 2008), defined as:

$$R_{\rho x} \equiv \frac{\beta \partial S/\partial x}{\alpha \partial T/\partial x}$$

where α and β are the thermal expansion and saline contraction coefficients, and $\partial S/\partial x$ and $\partial T/\partial x$ are the horizontal temperature and salinity gradients, respectively. The horizontal density gradient can be thought of as a normalized slope on the T-S diagram. The survey means and population standard deviations of the horizontal density gradient, from the layers within the central region on the T-S diagram, were found to be -0.12±0.27 in the 2012 survey, -0.29±0.36 in the 2013 survey, -0.02±0.37 in the 2014 survey, and -0.31±0.34 in the 2015 survey. Thus, scaled horizontal salinity variations are small in comparison to the horizontal temperature variations.

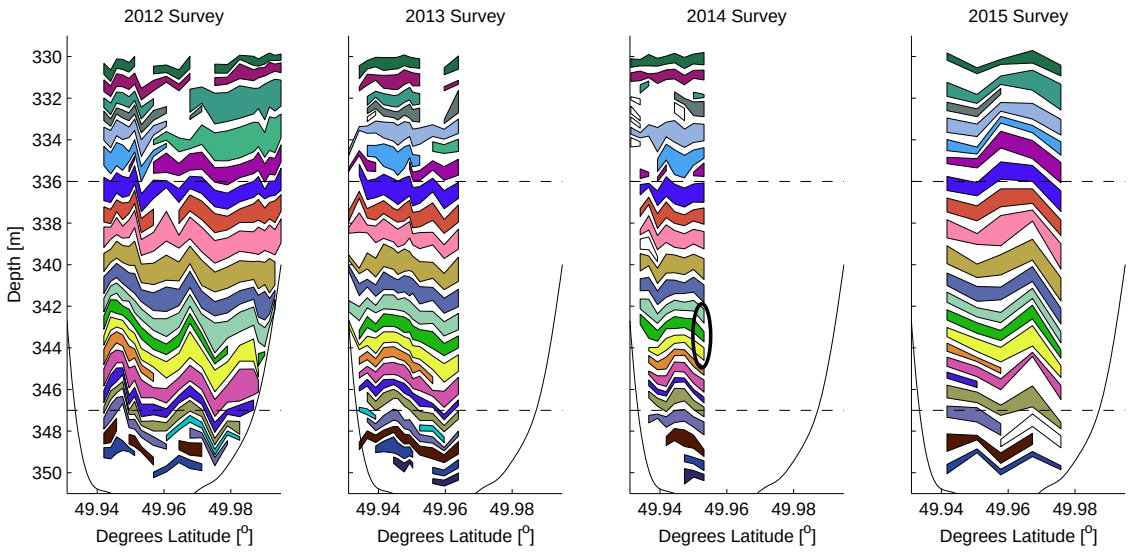

Figure 3.3: The depths and vertical thickness of the DD layers found in each survey. Colours indicate the layers matched up from year to year and the region between dashed lines indicate the central layers with the most coherent properties. Both the colours and the boxed region are consistent with those shown in Figure 3.2. Mooring location is shown as black ellipse in 2014 data.

The horizontal extents of the layers (Figure 3.3) indicate that many of the layers are coherent over the entire sampling domain of roughly 9 km, especially in the depth range of 336 m to 347 m. This region corresponds to the central region in the T-S diagrams, where the clusters are most evident. This section of the water column is characterized by near constant values of the vertical density gradient, $R_{\rho z} = 2.2 \pm 0.2$, and buoyancy frequency, $N = (2.3 \pm 0.3) \times 10^{-3}$ Hz (Figure 3.4). Above and below this depth range, the layers appear less coherent along the lake, clusters on T-S diagrams appear less compact, and the vertical density ratio and buoyancy frequency increase from their central region values. Although the Rayleigh number, Ra, has a maximum of $\sim 10^7$ in the central region, vertical variations in Ra do not correlate in an obvious way with the structure of $R_{\rho z}$ or N (Figure 3.4).

Variability in the depths of individual layers appears to be similar in neighbouring layers above and below. An example of this can be seen with the roughly 0.5 m rise in the layers present around a latitude of 49.97° in both the 2012 and 2015 surveys (Figure 3.3). There also exist sections in which layers appear to terminate away from the side boundaries. The most evident case of this can be seen with the layer around a depth of 345 m, which is bound by the layers above and below it, and terminates at a latitude of just under 49.96°. This layer termination can be seen in the 2012, 2013, and 2015 surveys; the 2014 survey did not capture data at this latitude.

The corresponding properties of the layers (Figure 3.5) indicate that the salinity is almost uniform along layers, consistent with the almost vertical clustering in Figure 3.2, whereas the temperature and density show consistent along-lake trends in their structure. The trends of the layer

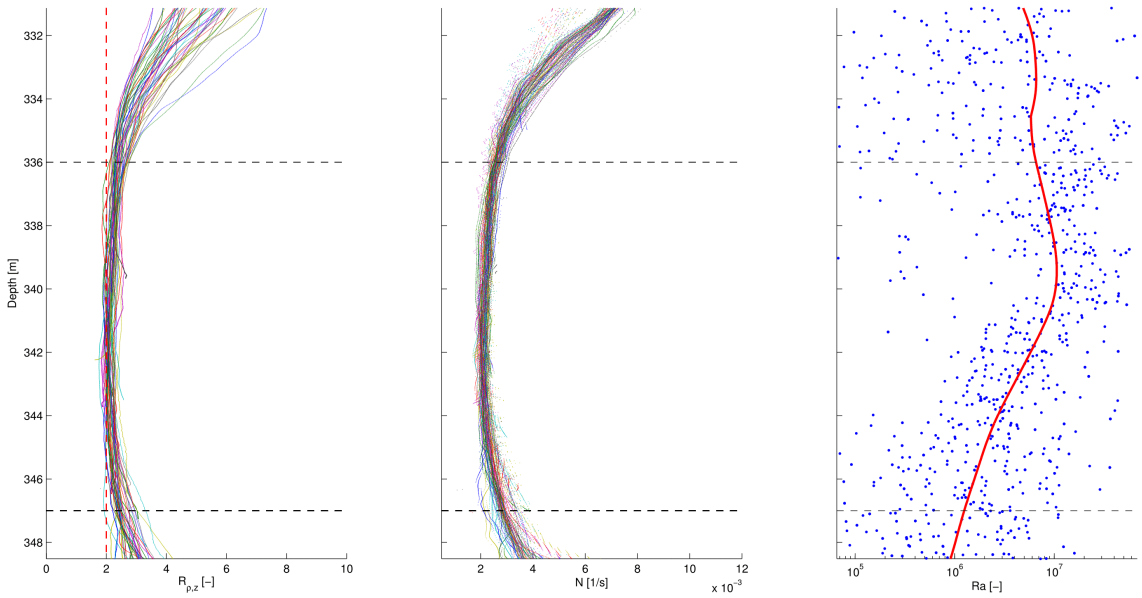

Figure 3.4: Left to right: The background vertical density gradient, $R_{\rho z}$, buoyancy frequency, N, and Rayleigh number, Ra, of all of the profiles from the 2012-15 surveys. Values of $R_{\rho z}$ and N are almost constant with depth in the central region between 336 m to 347 m. This structure is not visible in the Ra profile.

properties are most coherent among layers between depths of 336 m to 347 m, and less coherent in the layers outside of this central region.

Due to the consistency of the depth and temperature properties of the layers, it was possible to identify the same layers from year to year. This year-to-year existence of the same layers can be seen as consistent colours present in Figure 3.3 throughout each of the surveys, with unmatched layers left uncoloured. Once again, the layers in the central region were the most consistent; their properties did not change significantly from year to year, and the layers were identified with ease in successive years. In contrast, the layers above and below this region showed much more variation from year to year and were more difficult to track. The location of the October of 2014 mooring indicates that it was deployed in a region where the layers were relatively stable.

The deviations of the layer properties from their mean values were calculated in order to more clearly compare the layers from year to year. Deviations were first calculated for each layer, and then these deviations were averaged together for each survey (Figure 3.6). The mean deviations had to be shifted by +1 m°C in temperature, -0.2 mg/kg in salinity, and -0.3g/m^{3}in density to visually align with the results of the 2012 and 2015 surveys. The need for these shifts is attributed to the fact that the 2013 and 2014 surveys did not sample as much of the lake (horizontally), relative to the 2012 and 2015 surveys.

Linear least squares fits to the layer property deviations showed a general trend with layers getting colder by 2 m°C, more saline by 0.1 mg/kg, denser by 0.4 g/m^3, and deeper by 0.4 m from the southern to the northern ends of the 9 km lake bottom. These layer property variations

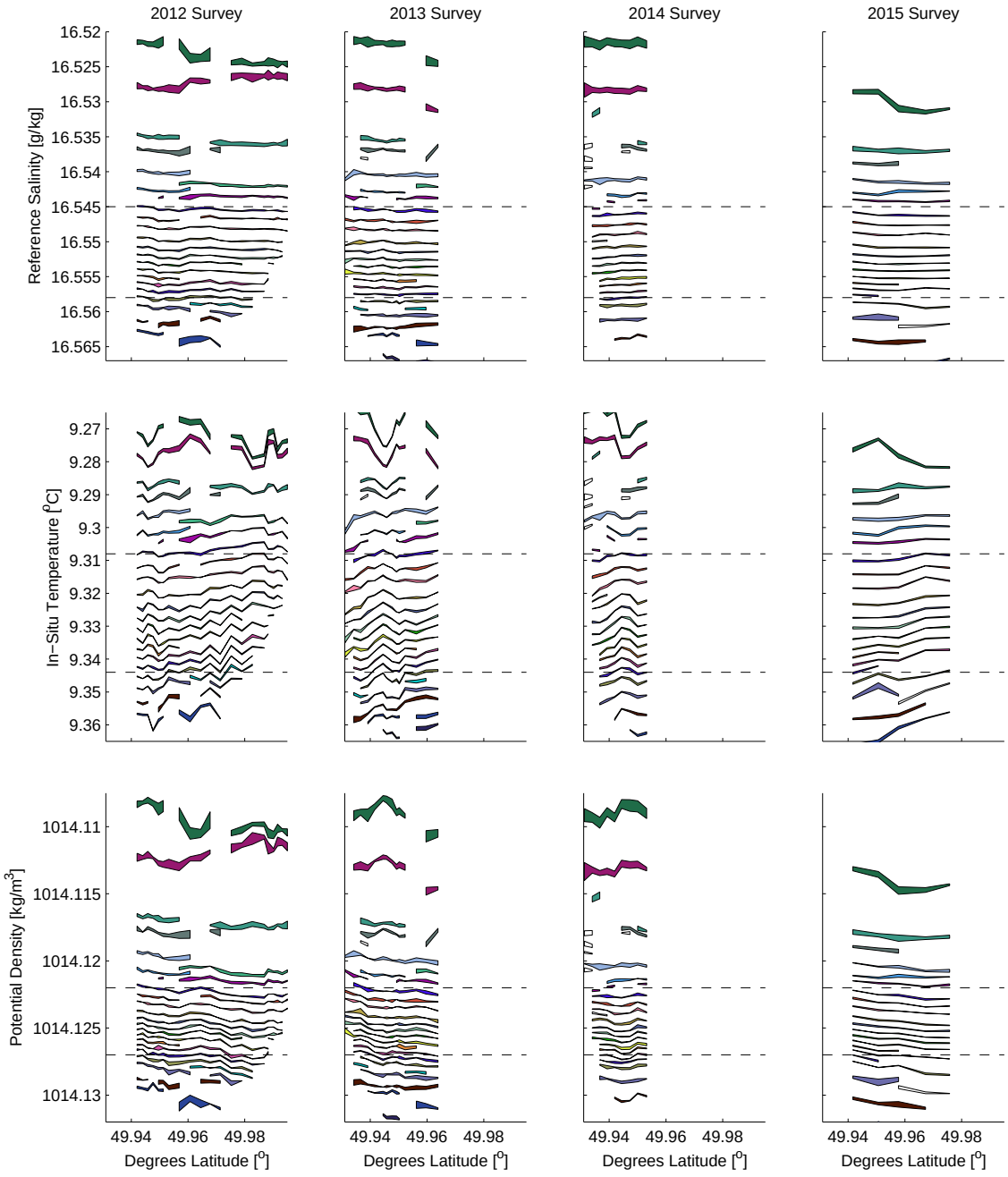

Figure 3.5: Top to bottom: Reference Salinity, in-situ temperature, and potential density (with a reference of 325 dbar) of the identified DD layers in each survey. Thicknesses of layer properties indicate the range of values between the lower and upper boundary of the step risers. Layer colours and central region between the dashed lines are consistent with those shown in Figure 3.2 and Figure 3.3.

.

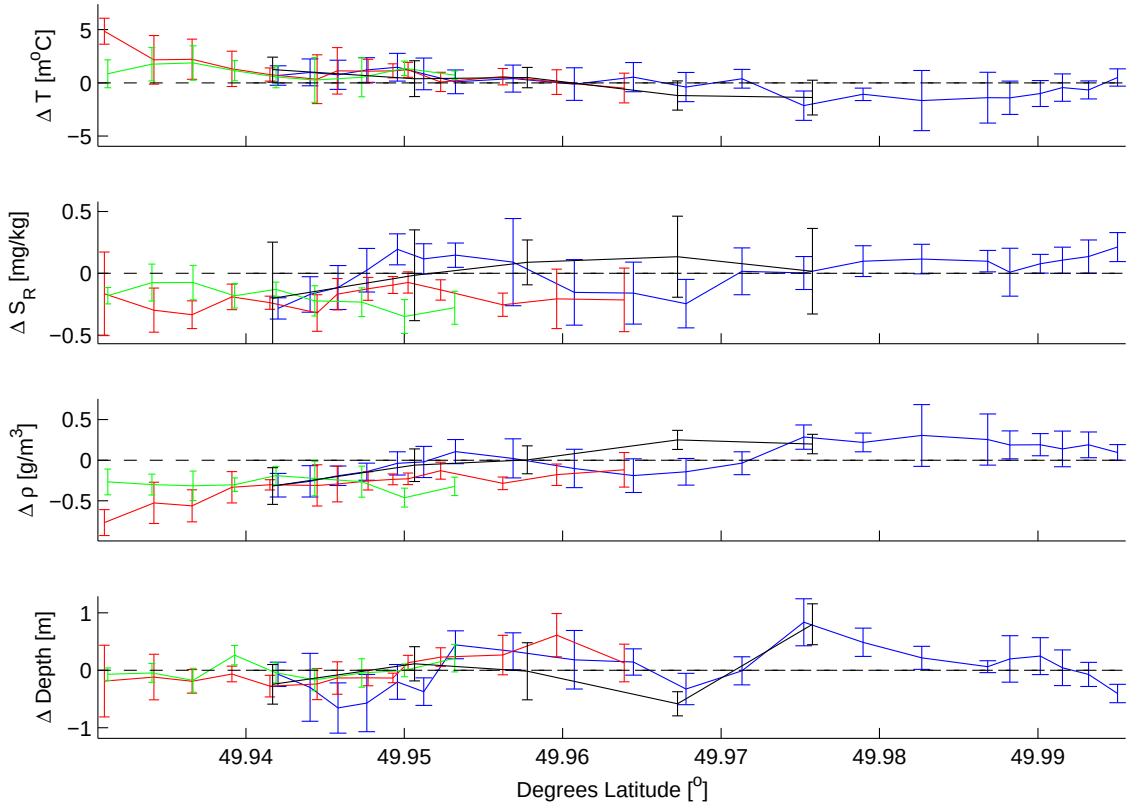

Figure 3.6: Top to bottom: Deviations of in-situ temperature, Reference Salinity, potential density, and depth of the layers from their layer mean values, averaged over all of the vertical layers in each survey. July 2012 survey shown in blue, June 2013 shown in red, May 2014 in green, and June 2015 in black. Error bars show the range of 1 sample standard deviation.

were smaller than the mean property differences between vertically adjacent layers (≈ 4 m°C and 2 mg/kg). Using the least squares fits to the temperature and salinity gradients, the horizontal density gradient, $R_{\rho x}$, was found to be -0.35$\pm$0.17 – an alternative approach to computing $R_{\rho x}$ by means of identifying the slopes of the layer clusters on a T-S plot. This approach is more reliable than the former since it incorporates the full horizontal extent and temporal evolution of the layers in its calculation.

3.2 Motions Within the Lake

The major feature of the observed currents were oscillations with a period of approximately 21 hours, with times of higher and lower activity over the deployment (Figure 3.7). The first few days of the mooring deployment showed high activity, followed by a calm period at the end of October/beginning of November. This was then followed by another high activity period of varying amplitude between November 2^{nd} and November 10^{th}. The least variable currents were observed between November 12^{th} and 22^{nd}, after which they became more active once again.

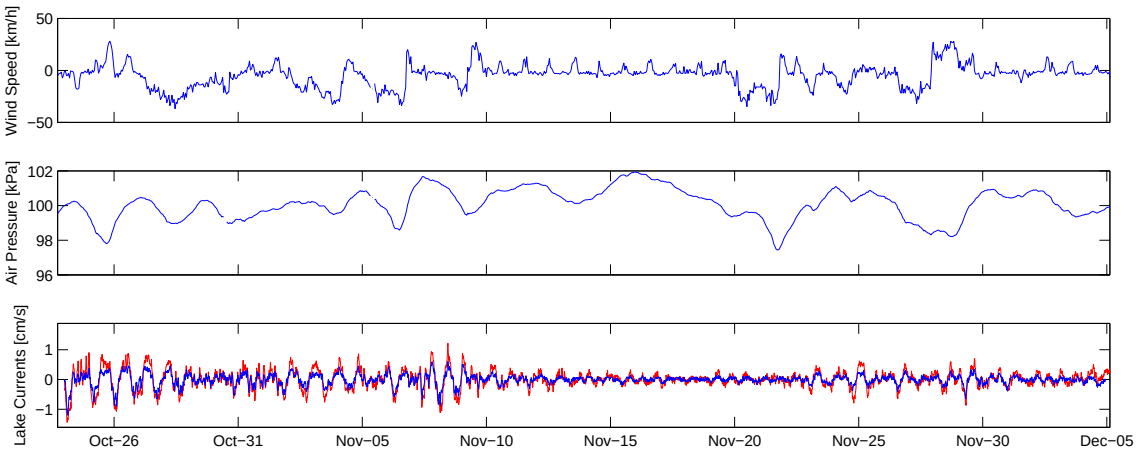

Figure 3.7: Top to bottom: Wind speed in the major axis direction of 165° (from the north-west); the air pressure; the lake horizontal currents speed obtained by the lower (blue) and upper (red) current meters with long term trends removed, 5-10 m above the lake bottom.

Wind and air pressure records were obtained from a government weather station at Powell River airport. The lake is roughly 10 km from the airport and surrounded by mountains on all sides, so that the airport records are probably not a good representation of the conditions over the lake. The wind and pressure data, however, showed similar trends in activity as those observed in the currents (Figure 3.7). More active winds and lower atmospheric pressures are seen around the time that the lake currents are most active, and higher pressures and calmer winds around the time when the currents are most quiet. There is also a time lag of a few days between changes in the activity of the winds/air pressure and the currents, which is likely due to inertia in the response. An analysis of the internal seiche modes present in the lake (not shown) suggested that the large current variations were most likely caused by wind activity coupling to an internal seiche mode with a period of approximately 21 hours. Maximum currents associated with the seiche activity are on the order of 1 cm/s.

In addition to the horizontal currents record obtained by the current meters, the arrangement of the temperature sensors on this mooring provided further information about the horizontal and vertical lake motions. The temperature record of the sensor located at 322 m depth, in a region of constant temperature gradient, varied in temperature by roughly ± 0.05°C, and in a manner similar to that of the currents obtained from the current meters (Figure 3.8, top right and Figure 3.7, bottom).

Since this sensor was in a region which was not DD active, the temperature gradient was nearly linear and could be used as a conversion between observed temperature and the vertical motion of the water column. The inferred motions showed vertical displacements of up to a metre above and below the initial depth (Figure 3.9, top), with similar variability as the horizontal displacements (of under 50 m) obtained from the integration of the along-lake currents (Figure 3.9, middle). These northward and downward (southward and upward) motions are highly correlated, which is consis-

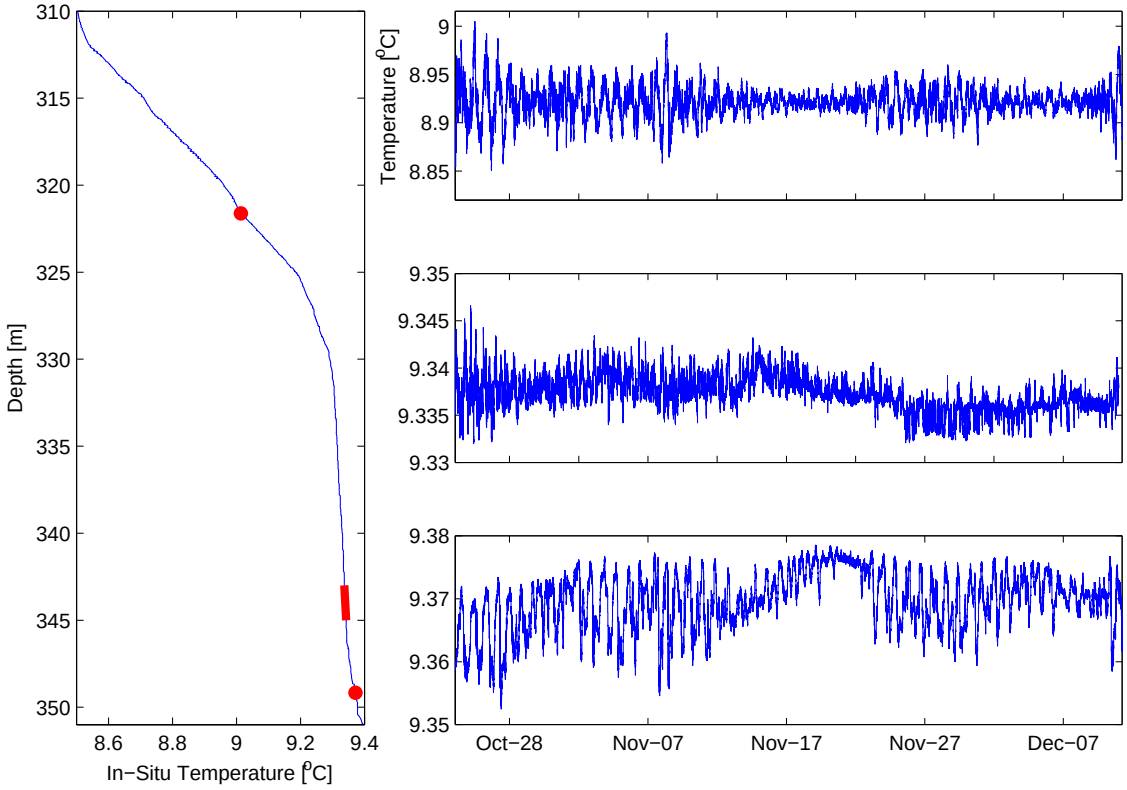

Figure 3.8: Left: The temperature profile of the bottom 40 m of the lake taken with the CTD profiler just before mooring deployment, indicating the locations of the three sections of temperature sensors (red circles). **Right:** The temperature record from: the temperature sensor at the 322 m depth (top); the middle temperature sensor on the 2 m long array of temperature sensors at a depth of 344 m (middle); the temperature sensor attached to the acoustic release, at a depth of 349 m (bottom).

tent with a seiche mode. The magnitude squared coherence spectrum of the two records (not shown) showed strong coherence in-phase in the 13-27 hour period range.

The temperature sensor on the acoustic release, 1 m above the lake bottom, showed temperature oscillations on the order of ± 0.03°C, similar to those seen at 322 m but with a varying long term trend (Figure 3.8, bottom right). This temperature series still exhibited the near daily oscillations common to the 322 m temperature sensor data and the current meter data, and showed a calm period with a peak temperature just after November 17^{th}, near the end of the period when the current deviation data showed the lowest activity.

Since the vertical motions near the lake bottom are presumably minimal and the geothermal heat flux is assumed to be constant in time over the sampling domain, the most likely remaining possibility for such temperature changes near the lake bottom would be a result of the horizontal advection of water with different temperatures. In order to match the scales of horizontal displacements inferred from this bottom temperature record with those obtained from the current meters, a horizontal temperature gradient of -0.1 m°C/m was assumed in the direction of motion (Figure 3.9,

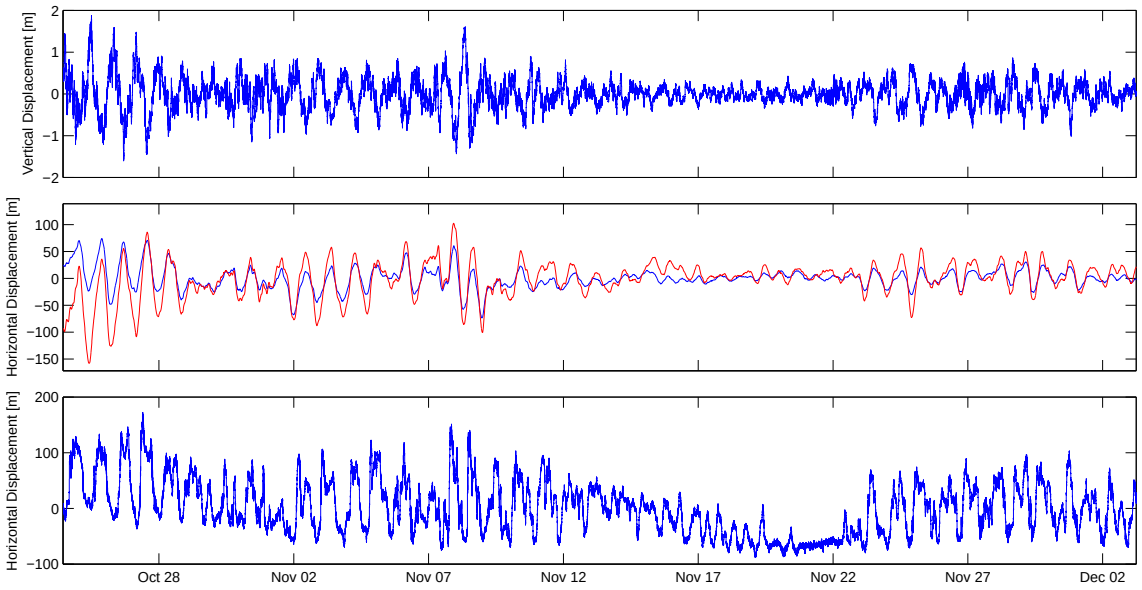

Figure 3.9: Top to bottom: Inferred vertical displacements of the temperature sensor at 322 m depth, using the CTD profiler data from the same region; the horizontal displacement of the lake water from the integrated currents from the lower (blue) and upper (red) current meter records; the possible horizontal displacement of the lake water from the temperature sensor at 349 m depth, assuming a horizontal temperature gradient of -0.1 m°C/m in the along-lake direction (northwest).

bottom) – along the major axis of the currents. This assumed horizontal temperature gradient is a factor of ~ 300 greater than the one obtained by looking at the four year mean temperature gradient within layers, which is roughly -3×10^{-4} m°C/m (Figure 3.6).

3.3 Dynamics Within a DD Layer

As was shown in the previous section, the mooring was regularly subjected to seiches on time scales of around a day. A vertical displacement of about 1 m at 30 m above the bottom suggests a vertical displacement of around 20 cm at 6 m above the bottom, but the observed vertical changes in the vertical temperature array are larger than this. These motions made it difficult to identify any DD steps in much of the temperature data (Figure 3.10, top) since these steps migrate outside of the sampling domain on a daily basis.

Also note that, although the temperature sensors were all corrected using calibration data, small offsets on the order of 0.5 m°C were still visible (Figure 3.10, top). These offsets appeared throughout the time series in the form of horizontal banding. To correct for this, a hyperbolic tangent function was fit to each step where they were identified, and deviations from this fit were corrected locally to remove these bands. This correction procedure was only applied when the time scale was on the order of a day and not more. Thus, the temperature data presented in Figure 3.10 still shows the banding features, but these sensor-related features have been removed in subsequent figures.

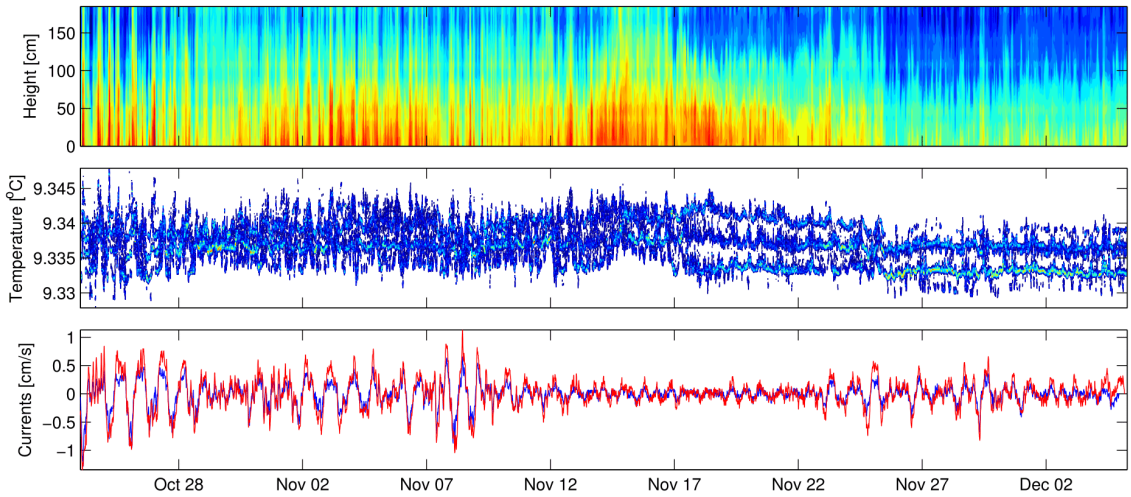

Figure 3.10: The October-December 2014 mooring data showing the contoured, post-calibration-corrected temperature record with height from the bottom sensor (top), the peaks of the temperature histogram time series (middle), and the 18-minute mean filtered currents in the along-lake direction from the lower (blue) and upper (red) current meters (bottom).

In order to more easily identify the DD steps present within the moored temperature data, the temperature time series was converted into a temperature histogram time series showing the dominant temperatures sampled at each time (Figure 3.10, middle). This method involved first interpolating the temperature data at each time step with a stiff spline to obtain a temperature profile with 1 cm vertical resolution, and then binning the data into 0.2 m°C bins to produce a temperature histogram time series. Since the convective region of a DD step has a near uniform temperature distribution, these regions could be found by looking at bins with a high count in the temperature histogram. Thus, the peaks in this temperature histogram time series would indicate the mean temperature within the step risers of any DD steps present, while the number of peaks would indicate the number of step risers, and thus the number of DD steps, present in the vertical-array data.

The number and consistency of DD steps found in the temperature record are related to the strength of the currents (Figure 3.10, bottom). During the first few days of the temperature record, when large oscillations occur in the horizontal current speeds, the steps appear and disappear repeatedly (Figure 3.11a). During October 25^{th}, between 12:00 and 21:00, no steps could be identified in the temperature data nor the temperature histogram peak data; the seiche currents are around 0.5 cm/s in the along-lake direction at this time. Between 21:00 on October 25^{th} and 03:00 on October 26^{th}, the currents reverse direction and four steps appear in both the temperature and temperature histogram data. Interestingly, the vertical position of the steps is affected by the two negative peaks in the currents just after 00:00 and around 02:30, producing a rise of nearly 50 cm of the steps. After 03:00 on October 26^{th} the steps once again appear to disintegrate as the currents reverse direction once more. The appearance and disappearance of the steps can be seen to occur twice more

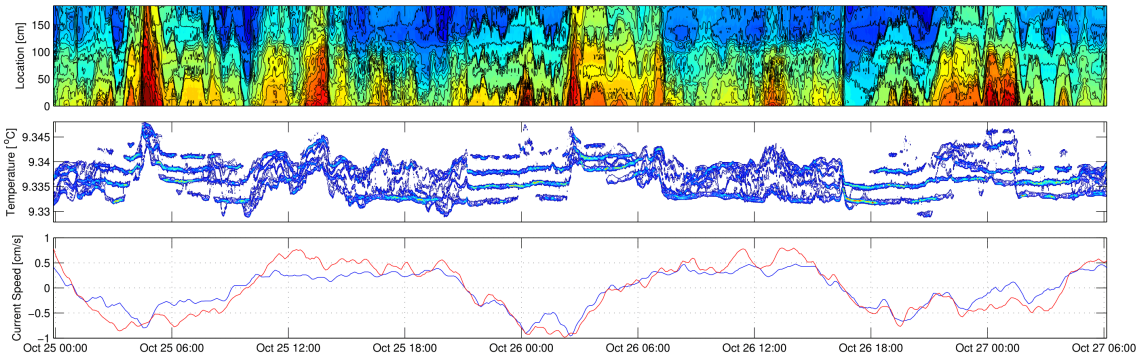

(a)

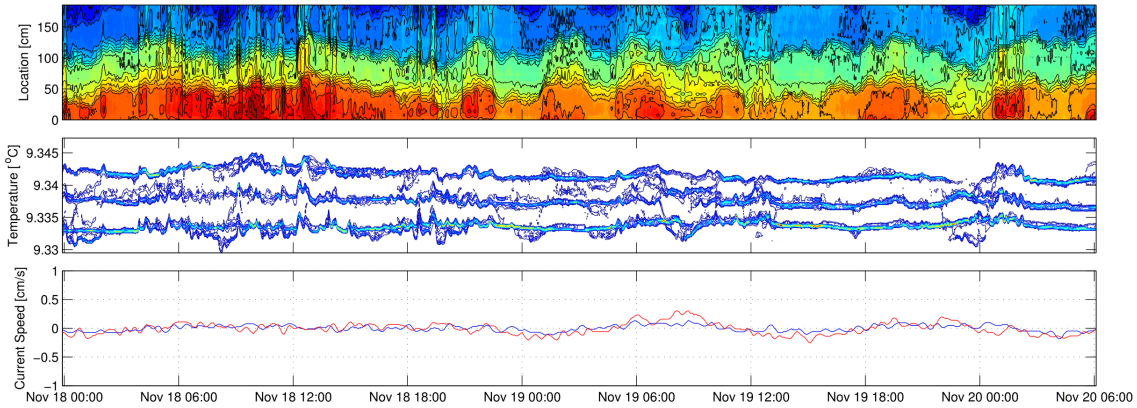

(b)

Figure 3.11: Periods in the moored time series when steps **a)** appear and disappear, and **b)** are fairly consistent in time, showing: the contoured temperature time series (top), the peaks of the temperature histogram time series (middle), and the 3 point running mean filtered currents in the along-lake direction (bottom).

in the 2 day period shown in Figure 3.11a, each time following the motions of the currents. It is therefore possible that this variability is actually spatial, with regions of formed and destroyed DD steps being advected past the mooring. Alternatively, since the mooring did not rotate during the deployment and the temperature sensors were all arranged on one side of the mooring, the observed step destruction could be the result of a wake generated by the presence of the mooring when the temperature sensors were facing down-stream of the currents.

Later in the mooring deployment, three steps could be consistently identified (Figure 3.11b). The formation of these three steps happens around the same time that the temperature maximum is reached in the bottom temperature sensor attached to the acoustic release – around November 17^{th}. During this period, the currents are weak, with speeds below 0.2 cm/s in magnitude, resulting in horizontal displacements of under 50 m. The steps migrate vertically by up to 50 cm during this period, but stay well defined in the temperature and temperature histogram data.

Since it allowed for the full identification of the middle step, bounded by the ones above and

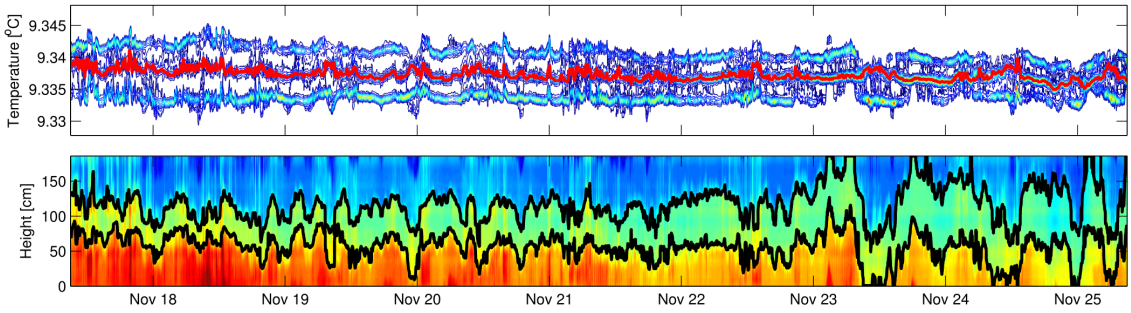

(a)

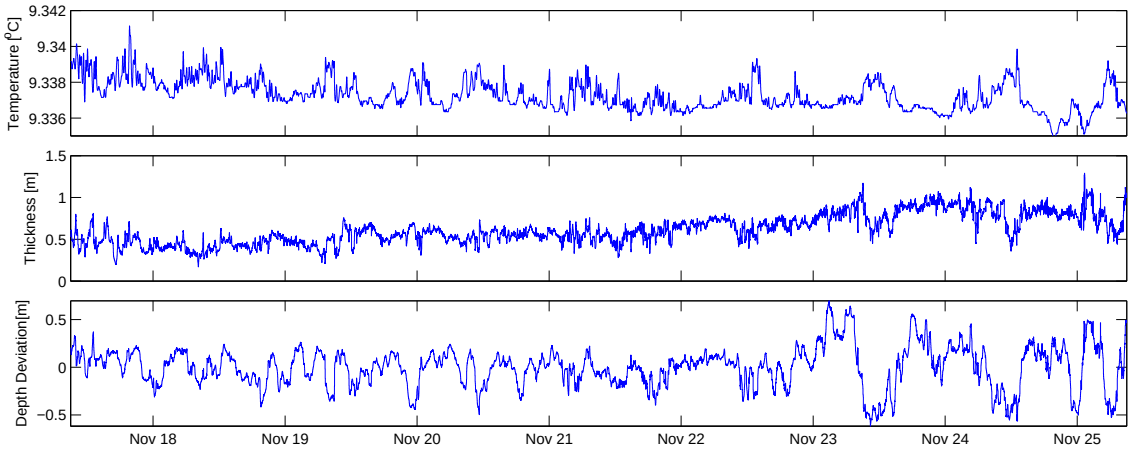

(b)

Figure 3.12: a) Location of a single DD step by means of isolating the step temperature (red line) using the temperature histogram time series (top), and then locating the corresponding upper and lower step boundaries (black lines) using the temperature time series (bottom). **b)** The evolution of the DD step properties for the period of time that the step was tracked.

below, this region was therefore used for the purposes of tracking the evolution of a single DD step. The central histogram peak was isolated, and the upper and lower limits of the step riser were located by identifying the places in the temperature time series (Figure 3.12a) where the temperature deviated by more than 1 m°C from the mean riser temperature. The step 'thickness' was defined to be the vertical distance between the upper and lower diffusive interfaces, and the step 'depth' as the mean of the depths of the two interfaces. During these 8 days the temperature of the step riser decreased by ~ 0.1 m°C, the depth stayed fairly consistent but fluctuated by up to ± 0.5 m, and the thickness increased from ~ 50 cm to ~ 90 cm before decreasing again (Figure 3.12b).

Although the horizontal velocities were not zero during this time, this period was the best time within the entire temperature record to examine processes in a reference frame fixed to the water mass in the step. In order to further understand the processes occurring within the DD step, the power spectra of the step riser properties and currents in this time period (between November 17^{th}

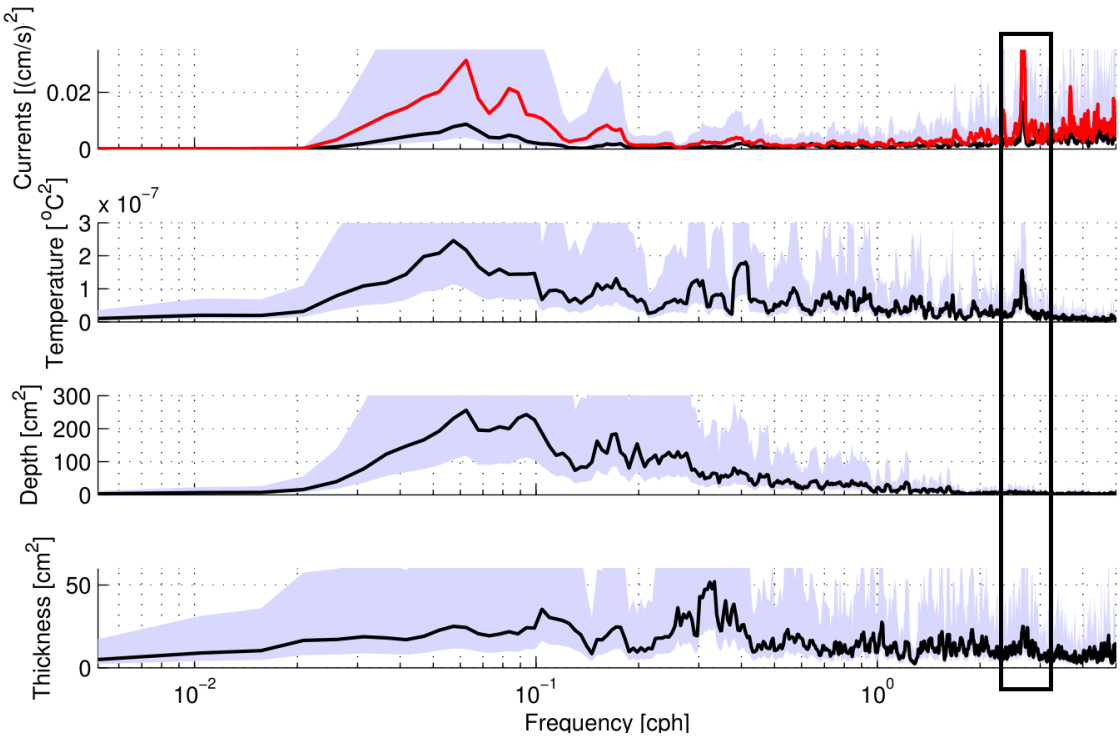

Figure 3.13: The variance preserving power spectra of the horizontal velocities and the DD step properties using the multi-taper method. Shaded regions show the 95% confidence limits. A common peak (shown within the boxed region) with a frequency of 2.73 cph is visible in the step temperature, currents, and step thickness.

and 25th) were computed by means of the multi-taper method (Figure 3.13). Although most of the variance in the data was found to occur in the low frequency regions (small seiche related motions), a common peak was observed in the high frequency end of the riser temperature, horizontal current speeds, and (not as strongly) DD step thickness spectra. This common peak had a frequency of $\sim$ 2.7 cph, resulting in a period of $\sim$22 minutes. This peak was not visible in the power spectrum of the depth of the step, implying that it is likely related to motions within the step (rather than of the entire staircase).

In order to see whether any features were visible on the time scale of the common peak found in the properties' spectra, the mean temperature record was band-pass filtered to isolate the 22 minute spectral peak (Figure 3.14), and two 6 hour regions were examined closely to show contrast between periods when the amplitude of the 22 minute signal was high (Figure 3.15a) and low (Figure 3.15b) (referred to as 'active' and 'less active' regions in what follows). Within the more active period in Figure 3.15a, higher temperature features are seen to appear periodically within the convective region of the step, either stretching from the bottom diffusive interface or appearing isolated in the centre of the convective riser; the less active period in Figure 3.15b does not show such features. This observation helps support the idea that the 22 minute spectral peak corresponds to thermal plumes within the convective riser, since such features are visible when the band-passed mean temperature signal is higher, and not visible when it is lower. During the 6 hour period on

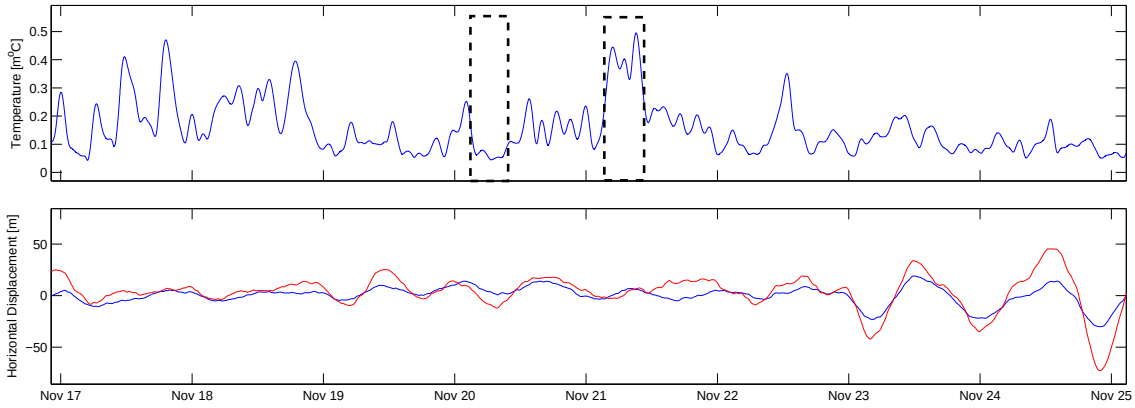

Figure 3.14: Top to bottom: The 22 minute band-pass filtered, mean temperature record from the 2-m vertical array, with the two chosen 6 hour periods (described in the text) indicated by dashed boxes; the horizontal displacement associated with the horizontal lake velocities from both current meters (upper current meter in red, lower current meter in blue).

November 21st, there were roughly 15 of these plume structures, appearing once every 24 minutes.

There was an asymmetry to the appearance of these plumes, such that warm plumes were consistently observed to extend upwards from the bottom diffusive interface, but no cold plumes were seen to extend downward from the upper diffusive interface. The plumes appear to (occasionally) have an effect on the layer thickness, stretching it upwards upon reaching the upper diffusive interface. This could explain the presence of the weaker (22 minute) peak in the step thickness power spectrum. At times, when powerful enough, the plumes appeared to penetrate into the step above and continue upwards (Figure 3.15a, around 07:00).

The variation in the band-pass filtered temperature record suggests that the plumes are intermittent features. It is possible that the plume formation is fixed spatially and that the advection of the water past the mooring (which is small but still non-zero) captures these sites periodically. However, no obvious correlation is present between inferred horizontal displacements and the strength of the band-passed mean temperature signal (Figure 3.14). Thus, it appears more likely that the variability is due to a temporal component rather than due to the advection of features from variable formation sites.

Based on the mean values of the band-passed temperature and horizontal velocity (not shown) records, the plume temperature anomaly and horizontal velocity scales were estimated as $T' \approx 0.2$ m°C and $u' \approx 0.5$ mm/s, respectively. Furthermore, by taking the $\sim$22 minute period of these plumes and the mean height of 0.6 m of a single DD step in this period, a vertical velocity scale of $w' \approx 0.5$ mm/s can be inferred.

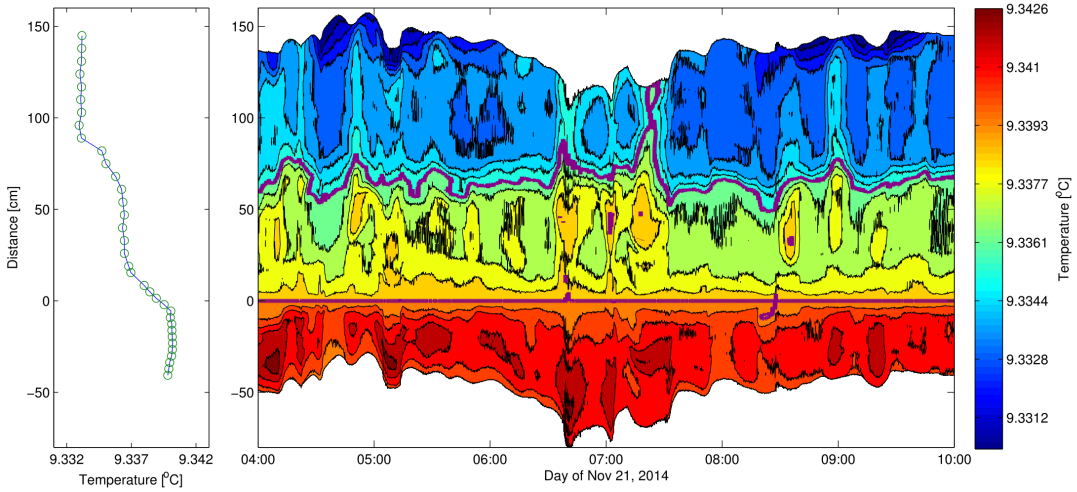

(a)

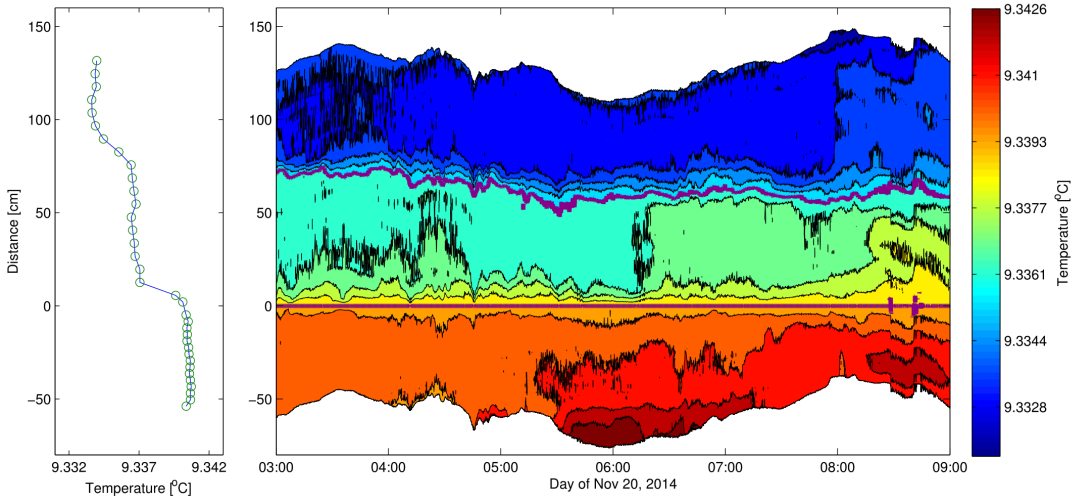

(b)

Figure 3.15: a) & b): The temperature profiles (left) as a function of distance from the bottom diffusive interface, at the initial time of the 6-hour close-ups (left) of the contoured temperature time series, when the DD step is clearly visible. Step boundaries are identified in purple, with the bottom interface fixed vertically in place to emphasize motions internal to the DD step.

Chapter 4

Discussion and Future Work

The diffusive mode of double-diffusive convection has been studied extensively using numerical and laboratory models. However, observations in natural systems have, in many ways, lagged behind. The present work addressed this gap by using observational data from the natural environment in Powell Lake, which allowed for a novel observation and characterization of the spatial and temporal processes of and within naturally occurring double diffusive layers.

The data attained from four annual surveys of vertical CTD profiles showed roughly 20 double-diffusive layers which were horizontally coherent throughout the entire lake and persistent over the four years. The moored temperature and horizontal velocity data revealed the presence of plume-like features in the convective region within an individual DD layer.

4.1 Convective Regime Within DD Layers

Previous laboratory studies have indicated that the convective regime within double diffusive steps varies depending on the local value of R_ρ, such that for $1 < R_\rho \leqslant 2$ the step is dominated by turbulent convection/mechanical mixing, and for $R_\rho > 2$ by intermittent thermal plumes emerging from the diffusive interfaces (Crapper, 1975; Lavery and Ross, 2007). Furthermore, it has been shown that the thickness of the diffusive interface has a tendency to increase for even higher values of R_ρ (Marmorino and Caldwell, 1976; Ross and Lavery, 2009), suggesting that the thermal plumes become weaker with increasing R_ρ.

Similar observations were made in numerical studies of the phenomenon, indicating that the convection regime consists of intermittent convective instabilities for $R_\rho > 2$ (Linden and Shirtcliffe, 1978), with three-dimensional effects (a signal of fully turbulent convection) only becoming present for $R_\rho \leqslant 2$ (Flanagan et al., 2013). Direct numerical simulation by Carpenter et al. (2012) indicated the presence of plume-like instabilities (at $R_\rho = 3$) which formed in the boundary layers of the diffusive interface.

In most laboratory studies the existence of thermal plumes has only been hinted at by the observation of fluctuations in the temperature signals with timescales of a factor of 1 to $\sim$10 times that of the buoyancy period, N^{-1} (Turner, 1968; Marmorino and Caldwell, 1976; Newell, 1984).

In contract, the laboratory studies of Lavery and Ross (2007) and Ross and Lavery (2009) showed the existence of plumes more definitively because of the use of acoustic techniques. In previous observational studies of naturally occurring DD structures, although there have been indications that the DD steps are indeed in a state of convection (Zhou and Lu, 2013; Schmid et al., 2010), the similarity of the convective regime to that observed in laboratory and numerical studies has only been suggested (Padman and Dillon, 1987). Thus, the observations in the present study provide a novel comparison between laboratory/numerical studies and observations of the convective regime within individual steps, and help validate some of the results of those studies.

Although it is observed that $R_{\rho z} > 2$ for the majority of the CTD profiles (Figure 3.4, left), roughly 6% of the data falls in the $R_{\rho z} \leqslant 2$ regime within the central depth range (between 336 m and 347 m). If the results from laboratory and numerical studies can be applied here, this would suggest that the majority of the DD layers in Powell Lake are stable in form, and are in a state of convection governed by intermittent thermal plumes, with occasional instances of more turbulent convection present within the layers at depths between 336 m and 347 m. This variability in the convective regime is consistent with the suggestion by Huppert (1971) that the stability (and thus the convective regime) of the DD layers is based on local conditions only, and so can vary for different locations within an individual layer.

The mooring was located in the central depth range, ideally placed to test this hypothesis. However, due to the presence of large-scale horizontal motions on the order of tens of metres (Figure 3.9) – which are most likely due to seiche activity produced by diel winds (Figure 3.7) – the moored instruments observed different regions within the lake throughout the sampling period. The fact that the layers appear clearly at some times and not others during the sampling period (Figure 3.11) suggests that either certain locations within the layer may be experiencing more active states of convection than others, or possibly that the presence of the mooring created occasional wakes which were able to disrupt the staircase structure. The spatial distributions of these regions could not be identified, however, because of the essentially one dimensional perspective provided by the moored data.

Luckily, the calm conditions during the period of November 17^{th} to 25^{th}, during which horizontal motions were minimal and a DD step could be observed consistently (Figure 3.10), allowed for a study of the dynamics within an individual DD layer (Figure 3.12)[1]. Of specific interest were the power spectra of the mean temperature within the convective region and the currents at this time, which show a common peak with a period of ~ 22 minutes (Figure 3.13). Unfortunately, the temperature and velocity signals could not be correlated directly because of the vertical offset between the location of the temperature sensors and current meters, but the agreement in periodicity suggests that the phenomena being captured are the same.

A common peak in the velocity and temperature spectra was also seen in a laboratory study of single component thermal convection by Qiu et al. (2004). In this study, the spectra of temperature

[1]A key assumption here, based on the calm conditions, is that the observed variability in the step properties are associated mostly with temporal effects rather than horizontal movement of the reference frame.

and velocity fluctuations at various points within a thermally driven convection cell were analyzed and a common peak was shown to exist, which was a result of the motions of the thermal plumes responsible for driving the convection within the cell.

Extrapolating these results from single component convection to the two component case leads to the interpretation of the common peak observed in this study as resulting from thermal plumes. The common peak period is a factor of 3 greater than the buoyancy period, which is in agreement with the predictions of Veronis (1965) for the period of the oscillations of these instabilities of $\sim$2 to $\sim$4.5 times that of the buoyancy period[2].

Band-pass filtering the temperature signal around this frequency and comparing it to the contoured temperature time series, it is observed that there appear plume-like features in the contoured temperature data (Figure 3.15). More plumes are visible when the amplitude of the band-passed temperature signal is larger, and less when the signal is smaller. The features in the contoured temperature data cannot be the result of the tilt of the mooring since the angle of the mooring never exceeded more than 1° from the vertical. The features are also unlikely to be solely caused by advected features since the 22-minute band-passed temperature record (which is an indicator of plume strength) did not show any obvious correlation to the horizontal displacements at this time (Figure 3.14).

A scale for the upward velocity of these plumes can be obtained by taking the product of the layer height, ~ 0.6m, and the plume frequency, $\sim 1/(22\times 60)$ Hz, resulting in a velocity scale of $w' \approx 0.5$ mm/s. A temperature scale for the plumes can be obtained from the mean value of the band-passed mean temperature signal, and results in a value of $T' \approx 0.2$ m°C. A similar procedure for the band-passed horizontal velocity time series results in a horizontal velocity scale of the plumes of $u' \approx 0.5$ mm/s.

Assuming that the known mean vertical heat flux, $F_H \approx 27$ mW/m^2 (Hyndman, 1976; Scheifele et al., 2014), is the resultant of plume activity only, and that the plumes' intermittency can be modelled by a sinusoid, results in a balance of

$$\frac{w'T'}{2}A' \approx \frac{F_H}{\rho c_P}A \tag{4.1}$$

where the factor of 2 on the left side comes from integrating $w'T'$ over one plume period, and A' and A are the cross-sectional areas associated with the plumes and the mean heat flux, respectively. Taking a typical value for the density to be $\rho \approx 1014$ kg/m^3, and the specific heat capacity of water to be $c_P \approx 4100$ J/(kg°C), results in $A'/A \approx 13\%$, indicating that the plumes cover $\sim 13\%$ of the area within the layers.

[2]The analysis by Veronis (1965) showed that the period of oscillations of these 'overstable' (as they were termed there) motions is $\sqrt{(1+Pr)}N_S^{-1}$ for short horizontal wavelengths and $\sqrt{5(1+Pr)}N_S^{-1}$ for long horizontal wavelengths, where $Pr \approx 7$ is the Prandtl number, and $N_S = \sqrt{g\beta\partial S/\partial z}$ is the buoyancy frequency based on the salinity gradient only. Using Equation 1.4 and Equation 1.5, these periods can be restated in terms of the buoyancy frequency, N, and the vertical density ratio, $R_{\rho z}$, as $\sqrt{(1+Pr)(1-1/R_{\rho z})}N^{-1}$ for short horizontal wavelengths, and $\sqrt{5(1+Pr)(1-1/R_{\rho z})}N^{-1}$ for long horizontal wavelengths. For a value of $R_{\rho z} = 2$, these periods equate to $2N^{-1}$ and $2\sqrt{5}N^{-1}$, respectively

4.2 Horizontal Coherence of DD Layers

Previous field observations of naturally occurring DD structures have indicated that staircase structures are often persistent over years (e.g. Hoare (1968), Carmack et al. (2012)) with layers that can be tracked horizontally for up to hundreds of kilometres in some instances (e.g Timmermans et al. (2008), Carmack et al. (2012)), but not in others (Sirevaag and Fer, 2012). The differences in these observations naturally leads to the question of what determines the horizontal coherence of these structures.

The observed DD layers in Powell Lake are consistently coherent over the length of the lake (Figure 3.3) and are surprisingly persistent over the four years of study, with the same ~ 20 layers identified in all four surveys. Not only are the layers themselves consistent, but their properties also appear quite steady over the course of the study (Figure 3.6), with the layers appearing consistently colder, saltier, and deeper towards the northern portion of the lake.

The horizontal coherence of the layers, however, is not the same at all depths. The central region (between 336 m and 347 m) consistently contains the most horizontally-coherent layers, spanning the entire lake length. The layer clusters on a T-S diagram are tightest in this central region – a feature that is similarly observed with the T-S clusters from the layers in the arctic (Timmermans et al., 2008). This region also exhibits a near uniform background vertical density ratio, $R_{\rho z} = 2.2 \pm 0.2$, and buoyancy frequency, $N = (2.3 \pm 0.3) \times 10^{-3}$ Hz (Figure 3.4, left); whereas the less horizontally-coherent layers both above and below this region show a larger value of $R_{\rho z}$ and N. Although the layer height varies horizontally along the layers, no layer merging or splitting is seen in the central region for the entire 4 year duration, suggesting that the layers are stable.

The value of $R_{\rho z} = 2.2 \pm 0.2$ for the stable layers in the central region is consistent with predictions from laboratory (Turner and Chen, 1974) and numerical (Huppert, 1971) studies, where it was observed that the layers would be stable provided that $R_{\rho z} > 2$. Furthermore, due to the stability of the layers, it can be inferred that they are in a regime for where the density flux ratio, γ, is at a constant value of ~ 0.15 (Radko, 2003). A typical value $R_{\rho z} = 2$ is accepted as the region for where γ transitions into this constant regime (Turner, 1968).

As the DD structure is in the intermittent plume regime of convection, and the strength of the plumes diminishes with increasing $R_{\rho z}$ (Newell, 1984), this could explain why the top and bottom layers (although still in the stable regime of $R_{\rho z}$) appear less coherent than those within the central region. The higher values of $R_{\rho z}$ in the top and bottom DD layers would imply that the plumes are weaker there, and are less able to maintain well defined diffusive interfaces. As such, without the containment provided by strong plumes, the interfaces would be more prone to diffuse (vertically) outwards and erode away, thus destroying the horizontal coherence of the layers.

Although layers become less coherent both above and below the central region, there are differences between the top and bottom layers. This is observed in the differences between layer clusters in T-S diagrams, where the clusters associated with the top layers tend to have a larger spread in temperature than those associated with layers at the bottom (Figure 3.2). The cluster trends observed in the arctic study by Timmermans et al. (2008) show similarity to those present at Powell

Lake, and suggests that horizontal coherence of the layers is variable in the arctic as well, with more horizontally-coherent layers sandwiched between less horizontally-coherent layers.

The difference between the two is further emphasized in the fact that the top layers are more horizontally-coherent than those at the bottom, with the top layers typically having a single break in the layer along the length of the lake, while bottom layers are more segmented (Figure 3.3). These differences between the layers at the two boundaries may suggest that $R_{\rho z}$ alone is not enough to characterize the convective regime within, and stability of, the DD layers. It was recently found by Scheifele et al. (2014) that (in the DD system in Powell Lake) for values of $Ra \gtrsim 10^6$ and $R_{\rho z} \gtrsim 3$, the ratio between the total heat flux to conductive heat flux within a layer, given by the Nussult number,

$$Nu = \frac{HF_H}{\rho c_P k_T \Delta T} \tag{4.2}$$

can be described as a decreasing function of $R_{\rho z}$; whereas for lower Ra and $R_{\rho z}$, Nu is dependent primarily on Ra.

The vertical variability of the layer Rayleigh number (Figure 3.4, right) indicates that the top layers typically have a higher Ra than the bottom layers. The top layers have a mean Rayleigh number of $Ra > 10^6$ and vertical density ratio of $R_{\rho z} > 3$, whereas the bottom layers have a mean value of $Ra \approx 10^6$ and $2 < R_{\rho z} < 3$. These differences may suggest that the top layers are in a regime where Nu is governed by $R_{\rho z}$ and the bottom layers are in a regime where Nu is governed by Ra.

In addition, the numerical study by Carpenter et al. (2012) indicated that the transition region from the convective regime to the double diffusive regime (and also into the stable regime) may have a dependence on the Rayleigh number. Carpenter et al. (2012) showed that the transition would occur at higher values of $R_{\rho z}$, for higher values of Ra. This leads to the conclusion that as $R_{\rho z}$ is increased, in order to keep the convective regime constant, Ra has to be increased as well, and implies that when comparing layers with similar values of $R_{\rho z}$, the layer with higher Ra will be in a stronger state of convection.

Thus it appears that the horizontal coherence of layers is dependent upon the convective regime within the layers, with the most horizontally-coherent layers having the lowest values of $R_{\rho z}$ and highest values of Ra, such that the convective regime is still within the region for where γ is constant. This possible Ra dependence on the convective regime may explain why the most coherent layers appear at higher values of $R_{\rho z}$ in other studies, as in the case of Lake Kivu where the most coherent layers are observed with values of $R_{\rho z} \approx 4$ (T. Sommer, personal communication) and $Ra \approx 10^8$ (Sommer et al., 2013).

The horizontally-coherence of the layers can be easily identified by observing the clusters formed on T-S plots, because the most horizontally-coherent clusters will be associated with the tightest clusters. If the horizontal coherence is indeed determined by the convective state within the layers, this would imply that the convective state could also be determined solely by the properties of the clusters on T-S plots.

4.3 Variability of DD Layer Structure

In laboratory studies of a salt stratified fluid heated from below, the DD layers that form are typically horizontal with no overall slope. The layers observed in Powell Lake, however, show consistent variability in their depths (Figure 3.3). Since there are no known sources of external waters (e.g. underwater springs) at these depths or anywhere around the lake, and the deviations of the layer properties are consistent over time (Figure 3.6) – which implies that internal wave and seiche activity aliased over the sampling period are not the cause of this variability – it is likely that the observed layer variability is mainly due to the slower double diffusive processes, perhaps in relation to spatial changes in bottom geometry or heat flux.

The identification of layers using closest profile-to-profile salinity to isolate the clusters present on the T-S plot (Figure 3.2) indicates that that the layers tend to follow closely the contours of background salinity. However, since within the layers the horizontal buoyancy gradient due to temperature is larger than that due to salinity ($|\beta \partial T/\partial x| > |\alpha \partial S/\partial x|$, since $|R_{\rho x}| < 1$) it is likely that it is actually the temperature field that drives the variability within the layers, and the salinity field only attempts to compensate. The layer depth and the background temperature distribution are consistent over the study period, suggesting they are linked to one another (Figure 4.1).

The depth variation of the layers appears to follow closely the geometry of the isotherms; raising in areas with relatively warmer temperatures[3]. The lake bottom appears consistently warmer in the southern end of the lake, with two warm regions around latitudes of $\sim 49.945^\circ$ and $\sim 49.967^\circ$; the layer depths mirror this variability by raising slightly above these two warm patches and having an overall downward slope towards the northern end of the lake.

A similar relationship between temperature distribution and layer slope was found in the two dimensional laboratory study by Turner and Chen (1974), where it was shown that aside from bottom heating of a salt stratified fluid, layers could be set up in (at least) two other ways: by introducing a physical slope to the system or by injecting water at one side with different temperature and salinity from (but same density as) the ambient fluid. Although seemingly very different approaches, the underlying mechanism leading to layer formation is identical: in both of these cases a horizontal gradient in temperature and salinity is established, and thus the iso-surfaces are not perfectly horizontal.

Turner and Chen (1974) also showed that the established horizontal gradients drive convection in the form of intrusion-like layers that propagate horizontally at a downward angle. After the layers propagate to fill the entire domain, the overall appearance of the layers is nearly equivalent to those seen in the bottom heating case apart from one key feature: the layers formed in this way are all sloped rather than aligned with the horizontal. Furthermore, the convection that drives the propagation of these layers is still persistent after they have filled the domain, so that there is an overall layer circulation such that the flow is downslope in the upper portion of the layer and upslope in lower portion of the layer (Figure 4.2).

[3]The correlation is not perfect since the horizontal within-layer variations in temperature (and salinity) are still non-zero (Figure 3.6)

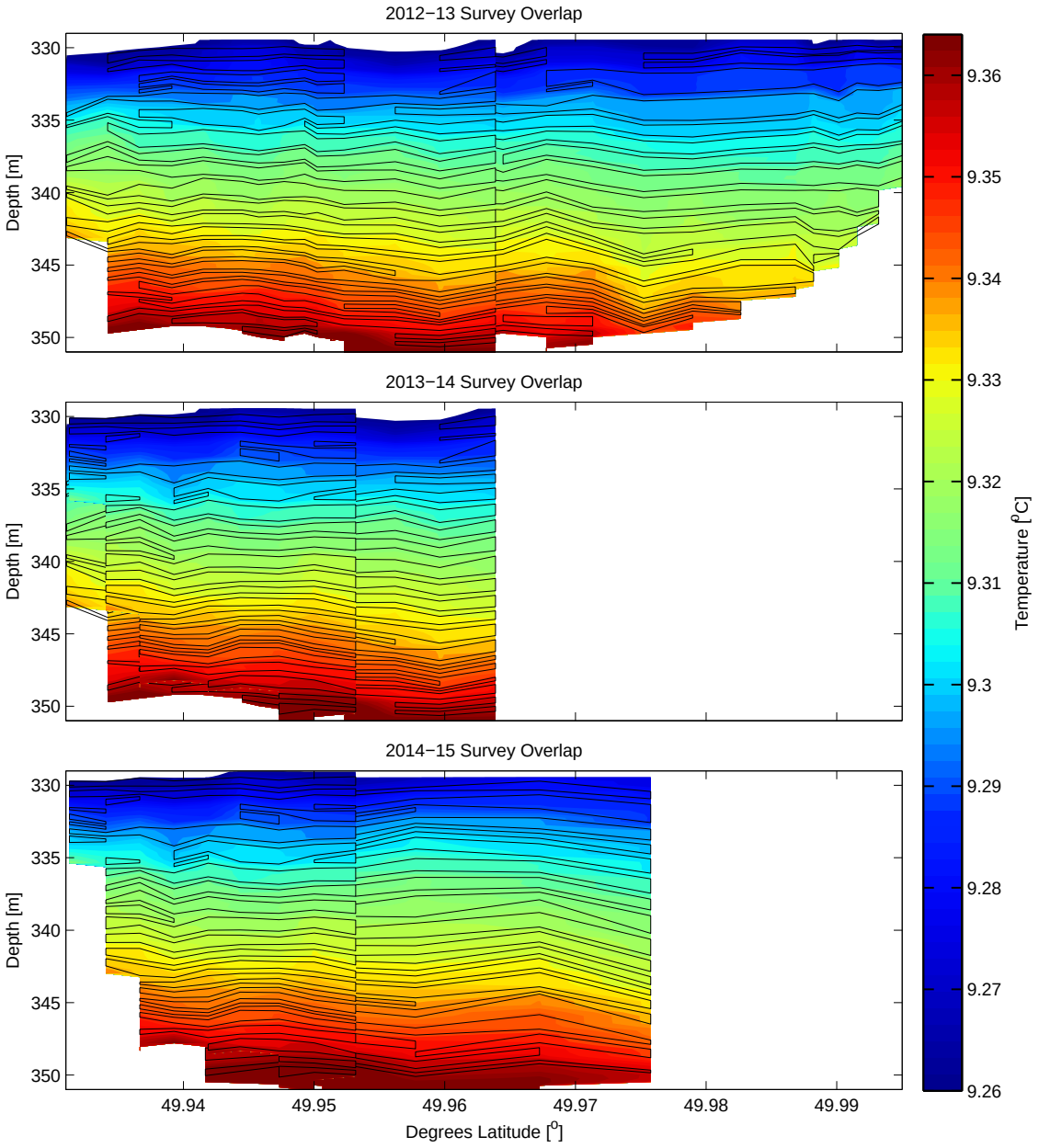

Figure 4.1: Outlines of overlapped DD layers from consecutive survey years, with 0.25 m vertically-binned background temperature in colour. Layers appear to be consistently raised in regions with relatively warmer waters. Note: 2015 data shifted downward by 0.3 m to better align with 2014 data.

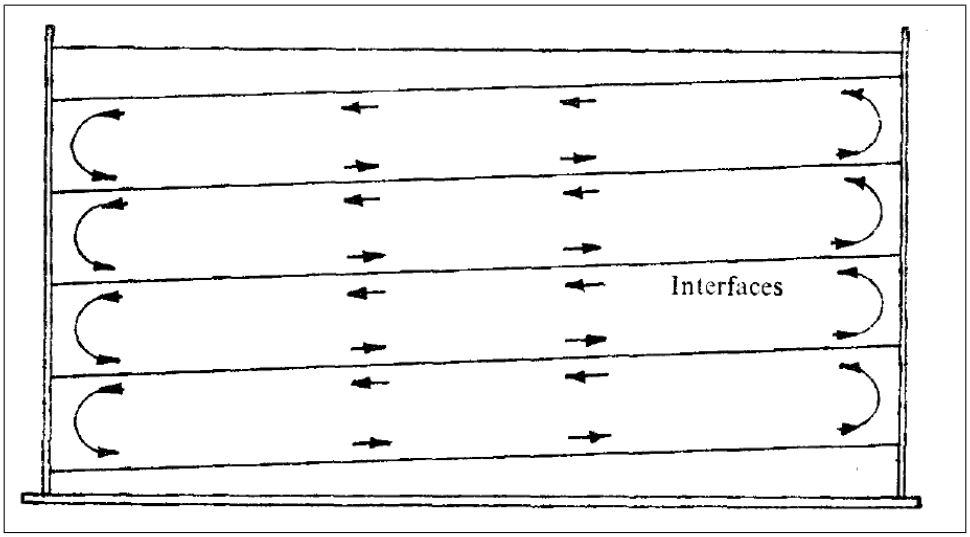

Figure 4.2: The circulation present within tilted layers. Adapted from Turner and Chen (1974).

The effects of a physical slope, and thus the iso-surface slope, were shown by Chen and Liou (1997) to play an important role in the formation of layers, affecting their number, structure, and thickness. An investigation on the sidewall heating of a two-layer salt stratified system by Bergman and Ungan (1988) indicated that the slope of the interface between the two layers was dependent on the applied horizontal temperature difference, suggesting that the slope of the DD layers would increase with higher horizontal temperature gradients (given equal horizontal salinity gradients). In both studies the convective circulation observed within the layers was identical to that observed by Turner and Chen (1974); similar circulation patterns were observed in naturally occurring DD staircase structures in the Arctic by Polyakov et al. (2012).

Thus, the angle of the layers is dependent upon the angle of the iso-surfaces of temperature and salinity, and angled layers would result in a characteristic layer circulation. The results from previous experiments also suggest that layers would be formed in regions where the layers show a peak in their depths, since layers tend to slope downwards away from their formation site. This would imply that in Powell Lake the layers are maintained primarily from the south side of the lake, but also around the two regions at latitudes of $\sim 49.945^\circ$ and $\sim 49.967^\circ$.

This could possibly explain the layer present at a depth of 345 m which is consistently seen to terminate at $\sim 49.958^\circ$. If the horizontal gradients differ between the two warmer regions at latitudes of $\sim 49.945^\circ$ and $\sim 49.967^\circ$, this would result in layers forming at those sites with different properties. It is plausible that more layers could be formed in the warm region at $\sim 49.945^\circ$ than the one at $\sim 49.967^\circ$. As the layers propagate outwards, the layers from each region would meet at the trough of the isotherm contour at a latitude of $\sim 49.958^\circ$. However, because of the differing number of layers formed at the two regions, a single layer would be left consistently unjoined. Merging might occur if the horizontal gradients were altered to be equal (but opposite in direction) at the two formation sites, so that the number of layers formed at each site would be the same.

In any layer where enough time has passed so that the system has stabilized to accommodate the

horizontal gradients, the temperature gradient would have an opposite sign to the salinity gradient (Turner and Chen, 1974). This would result in layers that appear warmer and less salty in raised sections of the layer, and colder and more salty in lowered sections of the layers, such that the layers would be most dense at their lowest point (and vice versa)[4]. These opposing gradients would imply that the the resulting value of $R_{\rho x}$ would be negative, which was shown to be the case for layers occurring in the Arctic (Timmermans et al., 2008), as well as in the present study of Powell Lake.

Furthermore, since horizontal gradients would occur only for sloped layers (and vice versa), a non-zero value of $R_{\rho x}$ would imply the existence of a sloped layer, with the magnitude possibly being related to the slope. Data of this sort is scarce, but a start is provided here showing that for a value of $R_{\rho x} = -0.35 \pm 0.17$, the observed mean layer slope is $\Delta z/\Delta x = 0.05 \pm 0.02$ m/km.

4.4 Summary and Future Work

The results of the present work indicate that the regime of $R_{\rho z} > 2$, with $Ra \approx 10^7$, consists of DD layers that are stable and do not merge, with a convective regime within the layers dominated by intermittent, buoyancy driven thermal plumes. These results are consistent with findings from numerical and laboratory studies of double diffusive systems, and suggests that other results from these studies can be carried over into the naturally occurring oceanic cases of double diffusive convection.

The horizontal coherence of the layers was consistent over the course of 4 years even when subject to persistent seiche activity, thus reinforcing the stability of these structures. The most coherent layers were observed in the central region of the domain, with a value of $R_{\rho z} = 2.2 \pm 0.2$; the less coherent layers were found above and below the central region with $R_{\rho z}$ values that were greater than those found in the central region. Qualitative differences between the layers above and below the central region with similar values of $R_{\rho z}$ but differing values of Ra implied that the most horizontally coherent layers would have the lowest (yet still stable) value of $R_{\rho z}$ with the highest Ra value, such that for two layers with equivalent values of $R_{\rho z}$, the layer with the higher Ra number would be more horizontally coherent.

The layers showed consistent variability in the layer depths and background temperature over the 4 years. The sloped sections of the layers appeared to be correlated with the presence of horizontal gradients of temperature and salinity, thus implying a relationship between $R_{\rho x}$ and the layer slope. Based on laboratory and numerical work, it is probable that due to the existence of a slope of the layers present at Powell Lake, there is a very slow large-scale along-layer circulation that would be occurring at the same time as the short scale convection due to the thermal plumes.

The presence of horizontal gradients suggests an altered picture for how the layers are formed and maintained within the environment at Powell Lake. Instead of the classic situation arising from from the case of the bottom heating of a salt stratified system – the development of a large initial convective layer at the bottom with subsequent layers developing one at at a time above that – the

[4] A subtlety present here is that the 'horizontal' gradients within the tilted DD layers would oppose one another, but the background horizontal gradients would still point in the same direction.

process here may rely on a slightly altered mechanism.

That is, due to the non-uniform temperature (and salinity) distribution present at the lake bottom, it is possible that the layers are formed/maintained via a method which combines the layer-upon-layer formation associated with bottom heating experiments, and the horizontal propagation of slanted intrusion-like layers associated with side heating experiments. Thus, the variability of the bottom temperature creates a situation where two dimensional effects become visible, primarily in the existence of a layer slope.

Testing this hypothesis for the layer up-keep mechanism at Powell Lake would require further study specifically including detailed profiling of the structure of the currents within the layers (which are presumable much smaller than the $\sim$0.5 mm/s velocity of the plumes), alongside more detailed study of the variability of the layer depths, to more accurately describe their geometry. Also, the relationship between $R_{\rho x}$ and the layer slope mights (in part) be determined from previous studies of naturally occurring layers where horizontal coherence has been found (e.g. Padman and Dillon (1987), Timmermans et al. (2008), Polyakov et al. (2012)).

Furthermore, laboratory and numerical studies could be performed on a bottom heated salt stratified fluid with a non-uniform bottom heat flux or bathymetry in order to better understand the relationship between the boundary heating conditions and the resultant layer geometry. Ideally, the circulation would also be determined within such systems so that the layer geometry, circulation, and background temperature/salinity distributions could be linked together.

Chapter 5

Conclusions

A study was performed in order to determine the spatial and temporal properties of naturally occurring double diffusive structures present at the bottom of Powell Lake. The aim of the study was to characterize the processes occurring on the scale of the overall layered DD staircase structure as well as within an individual DD layer, in order to compare the results with those previously obtained in numerical and laboratory studies of the phenomenon, and to validate the extrapolation of those results to oceanic observations. In order to achieve these aims, observations on the scale of the whole staircase structure were made by means of four annual surveys of cm-vertical and ∼300m-horizontal resolution CTD profiles along the 9 km length of the lake, and on the scale of an individual step by means of a month-long mooring consisting of thirty-eight temperature sensors and two current meters spaced vertically over 2 metres.

Within an individual DD layer, plume-like features were observed to be emitted intermittently from the lower diffusive interface. These features were observed to have a characteristic common peak in the power spectra of the mean temperature of the convective region and the horizontal currents. The period of this peak was found to be ~ 22 minutes, which is a factor of 3 higher than the buoyancy period, ~ 7 minutes, within that region. It was concluded that the convective regime within DD layers is composed of intermittent thermal plumes for a vertical density ratio of $R_{\rho z} = 2.2 \pm 0.2$, and Rayleigh number of $Ra \approx 10^7$. This is consistent with results from numerical and laboratory studies that show that the convective regime is composed of intermittent thermal plumes for the regime of $R_{\rho z} > 2$. The temperature scale for these plumes was estimated to be $T' \approx 0.2$ m°C, with associated vertical and horizontal velocity scales of $w' = u' \approx 0.5$ mm/s. Comparison with the mean vertical heat flux of 27mW/m^2 indicated that the warm upward-going plumes cover $\sim 13\%$ of the total area, so that the other $\sim 87\%$ is dominated by weaker downward-going colder flows.

DD steps within individual CTD profiles were identified and combined with those from adjacent profiles to form DD layers by means of isolating the clusters found on T-S diagrams, effectively matching up closest step salinity among adjacent profiles. The structure of the DD layers was observed to be consistent over the course of the entire study period and showed remarkable temporal persistence, as the same ~ 20 layers were tracked throughout all for years of study. The layers in the

central range (within depths of 336-347 m) were consistently horizontally-coherent over the entire lake length with near constant values of the vertical density ratio, $R_{\rho z} = 2.2 \pm 0.2$, and buoyancy frequency, $N = (2.3 \pm 0.3) \times 10^{-3}$ Hz, along with a peak in the Rayleigh number, $Ra \approx 10^7$. The layers above and below this region were observed to be less horizontally-coherent, with greater values of $R_{\rho z}$ and N. The top layers were more coherent than those near the bottom, suggesting that $R_{\rho z}$ is not the only parameter that determines the horizontal coherence of DD layers, and that given identical values of $R_{\rho z}$, layers with higher Ra are likely to be more horizontally coherent. The lack of observed layer merging over time in the central region indicates that for $R_{\rho z} = 2.2 \pm 0.2$ and $Ra = 10^6 - 10^7$ the layers are in a (quasi-) stable state. In this regime, the convective state within layers is strong enough to maintain well defined and horizontally-coherent layers, but not strong enough to cause those layers to become unstable.

The use of the closest profile-to-profile salinity as a criterion for isolating DD layer clusters on a T-S diagram indicated that the layers at Powell Lake tend to follow iso-surfaces of salinity. However, the depth variability of the layers also mimics the variability in the iso-surfaces of the background temperature, suggesting that layer depth is closely connected to the background temperature field. An implication of this is that DD layers are sloped in the presence of horizontal gradients of background temperature and salinity, and that the horizontal density ratio, $R_{\rho x}$, of the layers would be related to their mean slope, such that a non-zero value would indicate the presence of a sloped layer. It was shown that the temperature and salinity gradients along layers were persistent over the course of the study. Layers had a tendency to be colder by 2 m°C and saltier by 0.1 g/kg in the northern end, relative to the southern end of the lake. These layer gradients produce a horizontal density gradient of $R_{\rho x} = -0.35 \pm 0.17$, and are accompanied by a mean layer slope of $\Delta z / \Delta x = 0.05 \pm 0.02$ m/km. The fact that the layers are sloped and not perfectly horizontal would imply that there is a characteristic circulation within the layers, as seen in side heating experiments. This circulation should have the effect of homogenizing the spatial variation in the heat flux, so that layers further away from the (non-uniform) heating boundary should be less variable in their structure.

The results and suggestions presented in this study bring up several questions which lead to novel directions for the course of further study within the field of double diffusive convection, mainly dealing with the geometry of the formed layers and their relationship to background fields of temperature and salinity. In the case of Powell Lake, further work could be done to attain more precise measurements of the structure of the background temperature, salinity, and velocity fields, in order to determine precise relationships between those fields and the accompanying layer geometry. Previous field studies could also be revisited in order to determine if there is indeed a relationship between mean layer slope and the value of $R_{\rho z}$. Finally, laboratory and numerical studies could be incorporated by revisiting the standard salt-stratified heating experiments, except with non-uniform bottom heating or topography conditions to determine their effects on the geometry of the resulting DD layers.

Bibliography

Beckermann, C. and Viskanta, R. (1989). An experimental study of melting of binary mixtures with double-diffusive convection in the liquid. *Experimental Thermal and Fluid Science*, 2(1):17–26. → pages 8

Bergman, T. L. and Ungan, A. (1988). A note on lateral heating in a double-diffusive system. *Journal of Fluid Mechanics*, 194:175–186. → pages 44

Carmack, E. C., Williams, W. J., Zimmermann, S. L., and McLaughlin, F. a. (2012). The Arctic Ocean warms from below. *Geophysical Research Letters*, 39(7):1–6. → pages 6, 40

Carpenter, J. R., Sommer, T., and Wüest, a. (2012). Stability of a Double-Diffusive Interface in the Diffusive Convection Regime. *Journal of Physical Oceanography*, 42(5):840–854. → pages 8, 37, 41

Chen, Y.-M. and Liou, J.-K. (1997). Time-clependent double-diffusive convection due to salt-stratified fluid layer with differential heating in an inclined cavity. *International Journal of Heat and Mass Transfer*, 40(3):711–725. → pages 44

Crapper, P. F. (1975). Measurements across a diffusive interface. *Deep Sea Research*, 22(August 1975):537–545. → pages 4, 37

Flanagan, J. D., Lefler, A. S., and Radko, T. (2013). Heat transport through diffusive interfaces. *Geophysical Research Letters*, 40(10):2466–2470. → pages 8, 37

Hoare, R. a. (1968). Thermohaline convection in Lake Vanda, Antarctica. *Journal of Geophysical Research*, 73(2):607. → pages 6, 40

Huppert, H. E. (1971). On the stability of a series of double-diffusive layers. *Deep Sea Research and Oceanographic Abstracts*, 18(10):1005–1021. → pages 8, 38, 40

Hyndman, R. D. (1976). Heat flow measurements in the inlets of southwestern British Columbia. *Journal of Geophysical Research*, 81(2):337–349. → pages 12, 13, 39

IOC, SCOR, and IAPSO (2010). *The international thermodynamic equation of seawater - 2010: Calculation and use of thermodynamic properties*. Manual and Guides No. 56. Intergovernmental Oceanographic Commission, UNESCO (English). Available from http://www.TEOS-10.org. → pages 13

Kelley, D. E., Fernando, H. J. S., Gargett, a. E., Tanny, J., and Özsoy, E. (2003). The diffusive regime of double-diffusive convection. *Progress in Oceanography*, 56(3-4):461–481. → pages 2, 4

Kunze, E. (2003). A review of oceanic salt-fingering theory. *Progress in Oceanography*, 56(3-4):399–417. → pages 2

Lavery, A. and Ross, T. (2007). Acoustic scattering from ocean microstructure. *The Journal of the Acoustical Society of America*, 87(S1):S6. → pages 5, 37, 38

Lawson, K., Lemieux, B., Luck, J., and Woody, D. (1983). The development of a spherical, electromagnetic current meter. pages 187–193. → pages 18

Linden, P. F. and Shirtcliffe, T. G. L. (1978). The diffusive interface in double-diffusive convection. *Journal of Fluid Mechanics*, 87(03):417. → pages 8, 37

Marmorino, G. O. and Caldwell, D. R. (1976). Heat and salt transport through a diffusive thermohaline interface. *Deep Sea Research and Oceanographic Abstracts*, 23(1):59–67. → pages 4, 5, 37

Mathews, W. H. (1962). Bathymetry of Powell Lake, British Columbia. Technical Report 13, Institute of Oceanography, University of British Columbia. → pages 11

Mathews, W. H., Fyles, J., and Nasmith, H. (1970). Postglacial crustal movements in southwestern British Columbia and adjacent Washington State. *Canadian Journal of Earth Sciences*, 7(2):690–702. → pages 11

Nettelmann, N., Fortney, J. J., Moore, K., and Mankovich, C. (2015). An exploration of double diffusive convection in Jupiter as a result of hydrogen-helium phase separation. *Monthly Notices of the Royal Astronomical Society*, 447:3422–3441. → pages 8

Newell, T. a. (1984). Characteristics of a double-diffusive interface at high density stability ratios. *Journal of Fluid Mechanics*, 149(-1):385. → pages 4, 5, 37, 40

Noguchi, T. and Niino, H. (2010a). Multi-layered diffusive convection. Part 1. Spontaneous layer formation. *Journal of Fluid Mechanics*, 651:443. → pages 7

Noguchi, T. and Niino, H. (2010b). Multi-layered diffusive convection. Part 2. Dynamics of layer evolution. *Journal of Fluid Mechanics*, 651:465. → pages 8

Osborn, T. R. (1973). Temperature microstructure in Powell Lake. *Journal of Physical Oceanography*, 3:302–307. → pages 12

Padman, L. and Dillon, T. M. (1987). Vertical heat fluxes through the Beaufort Sea thermohaline staircase. *Journal of Geophysical Research: Oceans*, 92(C10):10799–10806. → pages 6, 21, 38, 46

Perry, K. and Pedersen, T. (1993). Sulphur speciation and pyrite formation in meromictic ex-fjords. *Geochimica et cosmochimica acta*, 57(18):4405–4418. → pages 12

Polyakov, I., Pnyushkov, A., Rember, R., Ivanov, V., Lenn, Y., Padman, L., and Carmack, E. (2012). Mooring-based observations of double-diffusive staircases over the Laptev Sea slope. *Journal of Physical Oceanography*, 42(1):95–109. → pages 6, 21, 44, 46

Qiu, X.-L., Shang, X.-D., Tong, P., and Xia, K.-Q. (2004). Velocity oscillations in turbulent RayleighBenard convection. *Physics of Fluids*, 16(2):412. → pages 38

Radko, T. (2003). A mechanism for layer formation in a double-diffusive fluid. *Journal of Fluid Mechanics*, 497(December 2003):365–380. → pages 8, 40

Radko, T. (2013). *Double-diffusive Convection*. Cambridge University Press. → pages 2

Radko, T. (2015). Double-diffusive convection, by timour radko. *Contemporary Physics*, 56(4):509–510. → pages 5

Rosenblum, E., Garaud, P., Traxler, a., and Stellmach, S. (2011). Turbulent Mixing and Layer Formation in Double-Diffusive Convection: Three-Dimensional Numerical Simulations and Theory. *The Astrophysical Journal*, 731(1):66. → pages 8

Ross, T. and Lavery, A. (2009). Laboratory observations of double-diffusive convection using high-frequency broadband acoustics. *Experiments in Fluids*, 46(2):355–364. → pages 5, 37, 38

Ruddick, B. and Gargett, A. E. (2003). Oceanic double-infusion: Introduction. *Progress in Oceanography*, 56(3-4):381–393. → pages 1

Sanderson, B., Perry, K., and Pedersen, T. (1986). Vertical diffusion in meromictic Powell Lake, British Columbia. *Journal of Geophysical Research*, 91:7647–7655. → pages 11, 12

Scheifele, B. (2013). Double diffusion in Powell Lake: New insights from a unique case study. Masters thesis, University of British Columbia. → pages 15, 16, 22

Scheifele, B., Pawlowicz, R., Sommer, T., and Wuest, A. (2014). Double diffusion in saline Powell Lake, British Columbia. *Journal of Physical Oceanography*, 44(2):2893–2908. → pages iii, v, 7, 12, 13, 21, 39, 41

Schmid, M., Busbridge, M., and Wüest, A. (2010). Double-diffusive convection in Lake Kivu. *Limnology and Oceanography*, 55:225–238. → pages 7, 21, 38

Schmid, M., Lorke, A., Dinkel, C., Tanyileke, G., and Wüest, A. (2004). Double-diffusive convection in Lake Nyos, Cameroon. *Deep-Sea Research Part I: Oceanographic Research Papers*, 51(8):1097–1111. → pages 7

Shirtcliffe, T. (1969). The development of layered thermosolutal convection. *International Journal of Heat and Mass Transfer*, 12(2):215–222. → pages 7

Sirevaag, A. and Fer, I. (2012). Vertical heat transfer in the Arctic Ocean: The role of double-diffusive mixing. *Journal of Geophysical Research: Oceans*, 117(7):1–16. → pages 6, 40

Sommer, T., Carpenter, J. R., Schmid, M., Lueck, R. G., Schurter, M., and Wüest, A. (2013). Interface structure and flux laws in a natural double-diffusive layering. *Journal of Geophysical Research: Oceans*, 118(11):6092–6106. → pages 7, 41

Stern, M. E. (1960). The "Salt-Fountain" and Thermohaline Convection. *Tellus A*, 1. → pages 1, 3

Stern, M. E. (1969). Collective instability of salt fingers. *Journal of Fluid Mechanics*, null:209–218. → pages 8

Timmermans, M.-L., Toole, J., Krishfield, R., and Winsor, P. (2008). Ice-Tethered Profiler observations of the double-diffusive staircase in the Canada Basin. *Journal of Geophysical Research*, 113. → pages 6, 22, 23, 40, 45, 46

Toffolon, M., Wüest, A., and Sommer, T. (2015). Minimal model for double diffusion and its application to kivu, nyos, and powell lake. *Journal of Geophysical Research: Oceans*, 120(9):6202–6224. → pages 7

Turner, J. (1965). The coupled turbulent transports of salt and and heat across a sharp density interface. *International Journal of Heat and Mass Transfer*, 8(5):759–767. → pages 3, 4

Turner, J. S. (1968). The behaviour of a stable salinity gradient heated from below. *Journal of Fluid Mechanics*, 33:183–200. → pages 3, 5, 37, 40

Turner, J. S. and Chen, C. F. (1974). Two-dimensional effects in double-diffusive convection. *Journal of Fluid Mechanics*, 63:577–592. → pages iii, v, 5, 40, 42, 44, 45

Veronis, G. (1965). On Finite Amplitude Instability in Thermohaline Convection. *Journal of Marine Research*, 23(1):1–17. → pages 39

von Rohden, C., Boehrer, B., and Ilmberger, J. (2010). Evidence for double diffusion in temperate meromictic lakes. *Hydrology and Earth System Sciences*, 14(4):667–674. → pages 7

Williams, P. M., Mathews, W. H., and Pickard, G. L. (1961). A lake in British Columbia containing old sea-water. *Nature*, 191:830–832. → pages 11

Zhou, S. Q. and Lu, Y. Z. (2013). Characterization of double diffusive convection steps and heat budget in the deep Arctic Ocean. *Journal of Geophysical Research: Oceans*, 118(12):6672–6686. → pages 6, 38

Zhou, S. Q., Qu, L., Lu, Y. Z., and Song, X. L. (2014). The instability of diffusive convection and its implication for the thermohaline staircases in the deep Arctic Ocean. *Ocean Science*, 10(1):127–134. → pages 6